Cell Reports

Resource

Sex shapes cell-type-specific transcriptional signatures of stress exposure in the mouse hypothalamus

Graphical abstract

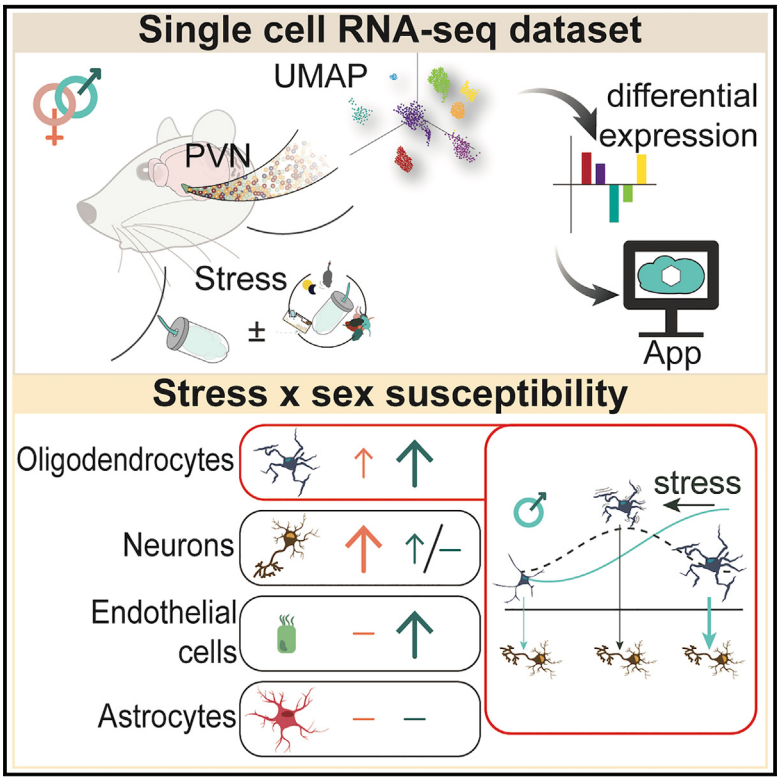

Highlights

- ARS elicits a cell-type- and sex-specific transcriptional response in the PVN
- Exposure to CMS influences the ability of different cell types to respond to ARS
- Oligodendrocytes are highly stress susceptible in a sex-specific way
- Male oligodendrocytes in the PVN have an altered maturation state after stress

Authors

Elena Brivio, Aron Kos, Alessandro Francesco Ulivi, ..., Mathias V. Schmidt, Juan Pablo Lopez, Alon Chen

Correspondence

jpablo.lopez@ki.se (J.P.L.), alon.chen@weizmann.ac.il (A.C.)

In brief

Brivio et al. generated a rich single-cell RNA sequencing dataset of the mouse paraventricular nucleus of the hypothalamus (PVN) to show that the response to acute stress is encoded differently in cell types and sexes. This approach identified oligodendrocytes as cells susceptible to stress.

Brivio et al., 2023, Cell Reports *42*, 112874
August 29, 2023
https://doi.org/10.1016/j.celrep.2023.112874

CellPress

Cell Reports

CellPress
OPEN ACCESS

Resource

Sex shapes cell-type-specific transcriptional signatures of stress exposure in the mouse hypothalamus

Elena Brivio,[1,2,3,4] Aron Kos,[1] Alessandro Francesco Ulivi,[5] Stoyo Karamihalev,[1,2,10] Andrea Ressle,[1] Rainer Stoffel,[1] Dana Hirsch,[6] Gil Stelzer,[7] Mathias V. Schmidt,[8] Juan Pablo Lopez,[1,9,*] and Alon Chen[1,3,4,11,*]

[1]Department of Stress Neurobiology and Neurogenetics, Max Planck Institute of Psychiatry, 80804 Munich, Germany
[2]International Max Planck Research School for Translational Psychiatry (IMPRS-TP), 80804 Munich, Germany
[3]Department of Molecular Neuroscience, Weizmann Institute of Science, Rehovot 76100, Israel
[4]Department of Brain Sciences, Weizmann Institute of Science, Rehovot 76100, Israel
[5]Department of Cellular Neuroscience, Leibniz Institute for Neurobiology, 39118 Magdeburg, Germany
[6]Department of Veterinary Resources, Weizmann Institute of Science, Rehovot 76100, Israel
[7]Bioinformatics Unit, Department of Life Sciences Core Facilities, Weizmann Institute of Science, Rehovot 76100, Israel
[8]Research Group Neurobiology of Stress Resilience, Max Planck Institute of Psychiatry, 80804 Munich, Germany
[9]Department of Neuroscience, Karolinska Institutet, 171 77 Stockholm, Sweden
[10]Present address: Department of Emotion Research, Max Planck Institute of Psychiatry, 80804 Munich, Germany
[11]Lead contact
*Correspondence: jpablo.lopez@ki.se (J.P.L.), alon.chen@weizmann.ac.il (A.C.)
https://doi.org/10.1016/j.celrep.2023.112874

SUMMARY

Stress-related psychiatric disorders and the stress system show prominent differences between males and females, as well as strongly divergent transcriptional changes. Despite several proposed mechanisms, we still lack the understanding of the molecular processes at play. Here, we explore the contribution of cell types to transcriptional sex dimorphism using single-cell RNA sequencing. We identify cell-type-specific signatures of acute restraint stress in the paraventricular nucleus of the hypothalamus, a central hub of the stress response, in male and female mice. Further, we show that a history of chronic mild stress alters these signatures in a sex-specific way, and we identify oligodendrocytes as a major target for these sex-specific effects. This dataset, which we provide as an online interactive app, offers the transcriptomes of thousands of individual cells as a molecular resource for an in-depth dissection of the interplay between cell types and sex on the mechanisms of the stress response.

INTRODUCTION

Stress-related psychiatric disorders, such as major depressive disorder (MDD) and anxiety disorders, are a major societal challenge due to their high prevalence and associated premature mortality.[1,2] Although they affect both men and women, they do not impact the sexes in the same way. Besides dissimilar prevalence, male and female patients display major differences in symptoms, comorbidities, disease progression, and treatment response.[3] These clinical differences are likely shaped by how sex modulates several biological processes underlying the disorders.[4] Although some of these processes are well studied, e.g., genetics and epigenetics, the memory processing system, the reward system, and the stress system activity,[5] the contribution of sex remains unclear. Understanding these differences is a prerequisite to develop effective treatments and provide efficient care to every patient.[6]

The hypothalamic-pituitary-adrenal (HPA) axis orchestrates the stress response and is involved in the pathophysiology of psychiatric disorders.[7] Chronic stress affects the ability of the HPA axis to respond to subsequent stress, and in turn, its dysfunctionality modulates the risk for stress-related psychiatric disorders.[7–9] The activity and sensitivity of the stress system and general stress perception[10] have observable sex differences.[4,11] These differences likely result from subtle variations in the molecular architecture of the male and female brain.[12,13]

Transcriptomic studies in several brain regions associated with the HPA axis have found a sex-specific response to stress exposure linked to depression, as well as sex-specific molecular mechanisms related to stress.[14,15] However, these studies used brain tissue homogenates, potentially diluting or minimalizing important cell-specific effects.[16] High-throughput technologies in single-cell transcriptomics now allow thousands of individual cells to be explored. Although there has been recent interest in employing this technology to explore sex differences in cell composition,[17,18] only a few studies have explored the idea that sex differences in stress and psychiatry might arise from the involvement of different cell types.[17,19,20] In this study, using single-cell RNA sequencing (scRNA-seq), we identified cell-type-specific signatures of acute stress in

the paraventricular nucleus of the hypothalamus (PVN) of male and female mice. We have generated a large resource dataset consisting of ~35,000 cells from sexually mature male and female mice following acute restraint stress (ARS) under baseline (naive) conditions or with a history of unpredictable chronic mild stress (CMS). First, we used a combination of bioinformatics and cellular approaches to characterize sex-specific transcriptional signatures of acute stress in different PVN cell types. Second, we showed that a history of chronic stress modulates the transcriptional signatures induced by acute stress and selectively affects individual cell populations in a sex-specific way. Finally, we identified a sex dimorphism in the stress sensitivity of oligodendrocytes, glial cells important for neuronal support and known to be altered in stress-related psychiatric disorders.

Overall, we provide a scRNA-seq dataset specifically designed for exploring sex differences after stress exposure in the PVN of adult mice. Our dataset provides a detailed characterization of sex differences in the stress response, which could support the development of sex-specific treatments and provide insights in the pathophysiology of stress-related psychiatric disorders. It constitutes a rich resource to identify cell- and sex-specific differences in response to stress (it is easily accessible through an interactive app available at https://male-female-stress.weizmann.ac.il/shinyApp/).

RESULTS

scRNA-seq captures the complexity of the PVN

To explore how different cell types of the PVN respond to acute stress exposure, we exposed sexually mature C57BL/6N male and female mice to a 15-min ARS. Before ARS exposure, the mice were kept either under baseline conditions (Baseline ARS) or were exposed to chronic stress (CMS ARS). This enabled us to investigate how sex and previous exposure to chronic stress modulate the ARS response. In addition, two non-stressed control groups (Baseline Control, CMS Control) were timely matched with each stress condition and used to generate a scRNA-seq dataset (Figure 1A). As expected, ARS generated a steep rise in blood corticosterone levels in both sexes (Figure S1A). To avoid any potential confounding effects from hormonal dysfunctions, only female mice without abnormalities in their estrus cycle (either prolonged or the absence of some stages; Figures S1B–S1D) were included. Overall, the majority (90.5%) cycled normally, with cycle-phase lengths similar to those observed by others[21] (Figure S1D).

Five hours after ARS, we generated single-cell suspensions from the extended PVN and used the droplet-based system from 10× Genomics to obtain scRNA-seq datasets of male or female cells. The eight individual datasets provided a total of 35,672 cells that passed quality controls (Figures 1B and S1E–S1G). Using linear dimensionality reduction followed by graph-based unsupervised clustering and Uniform Manifold Approximation and Projection (UMAP) for visualization, we identified a total of 33 distinct cell clusters, on which we mapped known gene markers for the PVN[22] (Figure S1H). In doing so, we classified cells into 17 identities: neurons (GABAergic, glutamatergic, GABAergic vasopressin [AVP], mixed), glia (astrocytes, macrophages [and microglia], oligodendrocytes [mature, committed oligodendrocytes precursors [COP], oligodendrocytes progenitor cells [OPCs]), and stroma (ependyma [ependymal cells, tanycytes], endothelium [endothelial cells, mixed endothelial], and perivascular [pericytes, vascular cells, and meningeal cells]) (Figures 1B and 1C; Table S1). By mapping markers associated to areas neighboring the dissected region (Figure S2A), we also evaluated the extent of non-PVN neurons included in our preparation (Figure S2B). Using the Allen Mouse Brain Atlas, we recognized some neuronal cells expressing markers of the neighboring regions: anterior hypothalamic area ($Pmch^+$), dorsomedial hypothalamic nucleus (Cck^+), medial preoptic area (Nts^+), medial preoptic nucleus ($Tac2^+$), suprachiasmatic nucleus ($Lhx1^+$), and ventromedial hypothalamus ($Nr5a1^+$). The presence of cells from areas lateral, caudal, and anterior to the PVN confirm that our dissection of an extended PVN captured the whole region, without biases between its more rostral and caudal parts.

To obtain a higher resolution of the neuronal complexity of the PVN, we further isolated GABAergic, glutamatergic, and mixed neurons and re-clustered them independently (Figure 1D). As a result, GABAergic neurons were split in 10 subpopulations, identified mainly by one or two marker genes (Figure 1E). For instance, we identified three different subgroups of Avp neurons (clusters 2, 3, and 5), two of which closely cluster in the hierarchical tree analysis (Figure 1D, right), reminiscent of two original Avp populations (Figure 1B). In addition, neuropeptides (*Tac1*, *Tac2*, *Vip*) or neuropeptide-associated genes (*Vgf*, *Scg2*) strongly contributed to the clustering of subpopulations of inhibitory neurons (Figures 1D and 1E). This subdivision was consistent with previously described hypothalamic clustering.[17,23] In our dataset, this was less true for glutamatergic neurons. Although in excitatory neurons we found the expression of *Trh* and *Crh*, neuropeptides characteristic of the PVN, in cluster 4 the rest of the clusters were mostly described by signaling molecules (*Calbn2*, *Pcp4*, *Ntng1*, *Tcf7l2*). Finally, the mixed neuronal subcluster 2 was defined by the expression of the pre-peptide *Cartpt*, a gene previously associated to hypothalamic neuronal subpopulations.[17,24]

Because many of these neuropeptides are expressed at very high levels, they often show background expression in droplet-based preparations and might confuse the detection of these populations.[22,25] To verify the extent of this contamination, we used discarded empty droplets to calculate the average expression of all genes in the ambient RNA (Table S2). As expected, we did find small contamination levels, especially of the two most abundant peptides of the PVN: *Avp* and *Oxt* (Figure S1C). However, specialized subtypes of neurons enriched in the PVN, such as the *Avp*, *Oxt*, *Sst*, *Trh*, and *Crh*-expressing neurons, could be easily identified by their clear expression above ambient levels (Figures S1D–S1H). Indeed, these neuropeptides were important leaf determinants in the hierarchical clustering (Figure 1D) and marked a specific subpopulation of reclustered neurons (Figure S2I).

Overall, our dataset captured the entirety of the PVN, with small inclusions of the neighboring regions, and the neuronal and non-neuronal complexity of several cellular subtypes.

CellPress
OPEN ACCESS

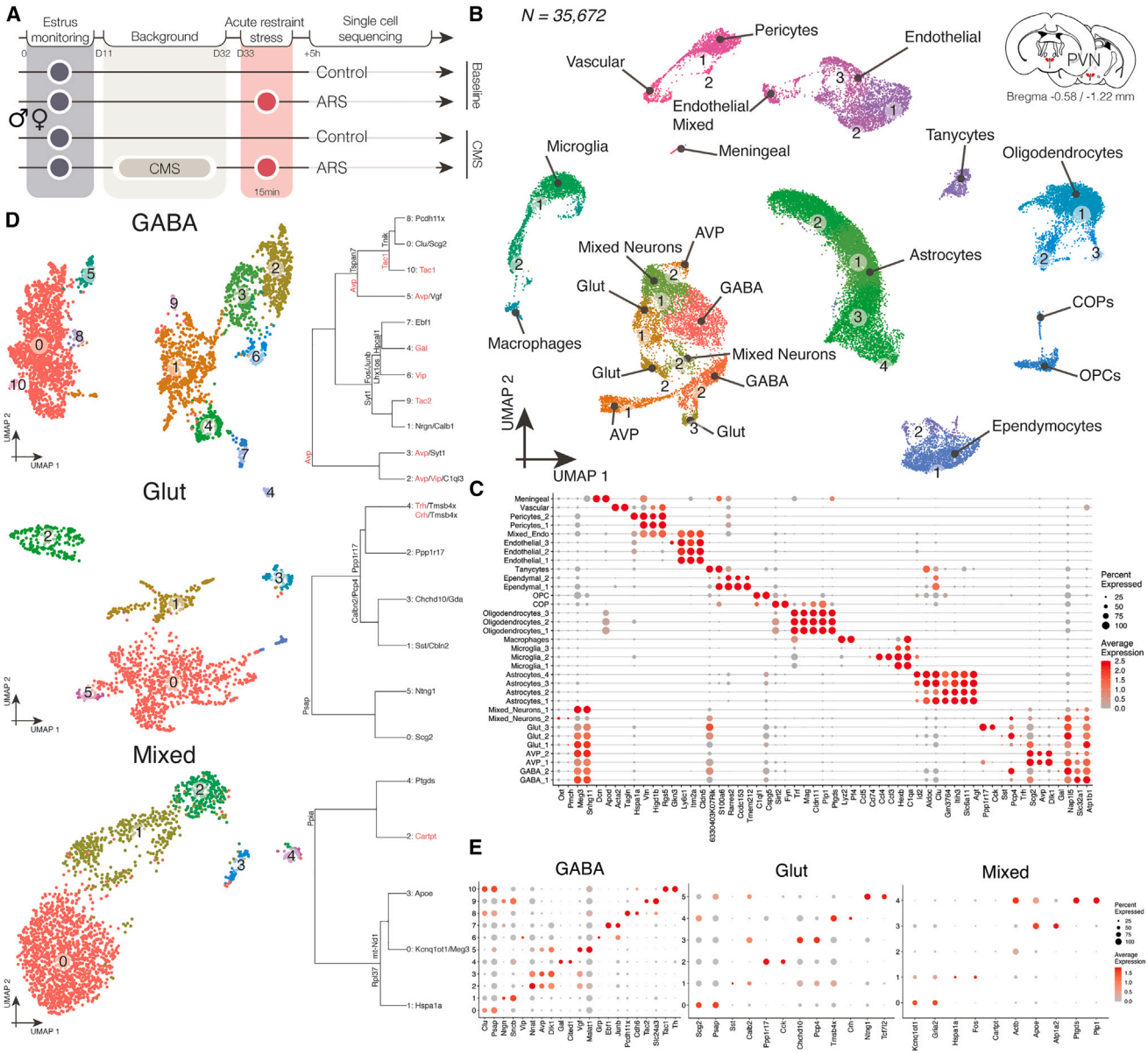

Figure 1. Overview of the experimental design and scRNA-seq dataset

(A) Experimental design of scRNA-seq. Mice underwent 3 weeks of unpredictable chronic mild stress (CMS) or home-cage housing (baseline) before 15-min acute restraint stress (ARS). The paraventricular nucleus of the hypothalamus (PVN) was processed for scRNA-seq 5 h post-ARS.

(B) Uniform manifold approximation and projection (UMAP) plot of 35,672 single cells. Numbers label subclusters.

(C) Heatmap showing the top two representative genes per cluster.

(D, left) UMAP plots of reclustered GABAergic (top), glutamatergic (middle), and mixed (bottom) neurons. (Right) Hierarchical trees for each subgroup. Some genes differentially expressed between tree nodes are shown. Neuropeptides are shown in red.

(E) Heatmap of the top two markers per cluster for each of the reclustered neuronal groups.

See also Figure S1 and Tables S1 and S2.

The transcriptional response to ARS is sex and cell type specific

To explore whether sex may modulate the transcriptional response to an acute stressor in the PVN, we characterized a normal acute stress response for each sex for each of the major cell types identified before (Figure 1A, Baseline ARS). Differentially expressed genes (DEGs) were identified using the Model-based Analysis of Single-cell Transcriptomics (MAST) algorithm. Overall, we found several DEGs in both sexes. Interestingly, females showed 1.5 times more DEGs than males (479 vs. 325) and a limited overlap of 137 genes (17% of all DEGs; Figure 2A). These overlapping genes were enriched for interactors of

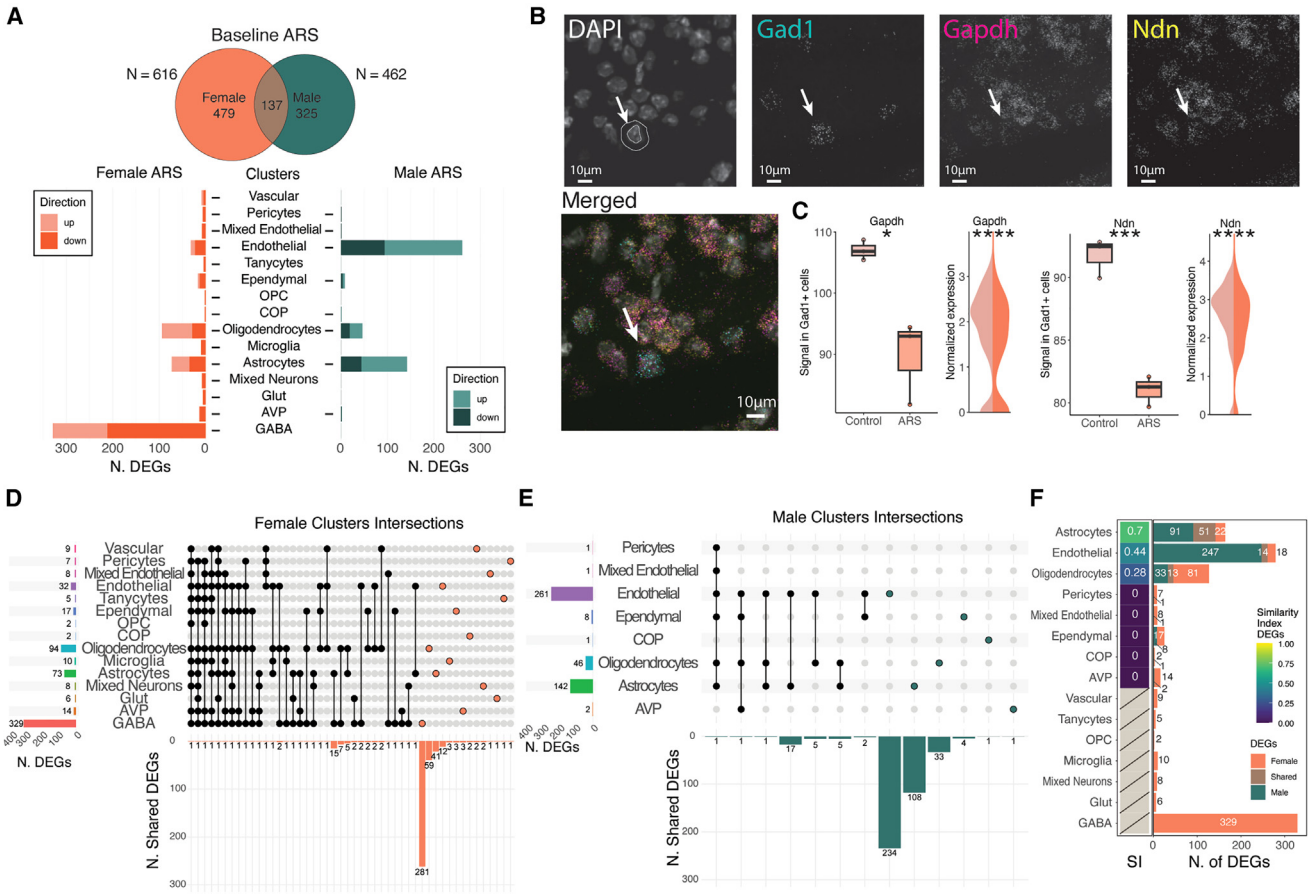

Figure 2. Transcriptional response to ARS at baseline

(A, upper) At baseline, females have more total DEGs after ARS than males (female = 616, male = 462 DEGs) with limited overlap (n = 137). (Lower) Distribution and directionality of DEGs is specific to the cell type and sex.

(B) Representative RNAscope images for GABAergic genes (scale bar, 10 μm). Arrows show an example GAD1$^+$ cell; white lines show the nucleus and cell regions of interest (ROIs) identification.

(C) Quantification of *Gapdh* and *Ndn* expression change caused by ARS in female *GAD1*$^+$ cell. Boxplots show RNAscope quantification by number of puncta; violin plot shows scRNA-seq results (t test, Gapdh: t(1) = 17.74, p = 0.013; Ndn: t (1) = 87.75, p = 0.0007). Boxplots: interquartile range (IQR) and median; whiskers: minimum and maximum value ± 1.5 IQR.

(D and E) UpSet plots of DEGs for (D) female and (E) male ARS response at baseline showing limited overlap between cell types. Barplot represents the number of genes shared across clusters identified (black dot and lines). Colored dots highlight group of DEGs unique to each cluster. Left panels show total number of DEGs for each individual cell type.

(F) Similarity of the ARS response between male and female clusters. (Left) Clusters ranked by similarity index (Szymkiewicz-Simpson coefficient). (Right) Absolute numbers of DEGs for male, female, or shared.

See also Figure S2 and Table S3.

transcription factors such as *Esr1*, *Atf2*, *Ilf3*, *Htt*, *Ctnnb1*, *Nfkb1*, and *Nr3c1*, all known to be major players in the response to stress[26] (Figure S3A).

Importantly, we found that the transcriptional response to acute stress is encoded in different cell types of the brain with a combination of upregulated and downregulated genes (Figures 2A, 2D, and 2E; Table S3). Fifteen clusters in females and eight in males had at least one DEG. Most of these responses were largely unique to the cell type (Figures 2D and 2E, colored dots), and only a few were shared between them (Figures 2D and 2E, black dots and lines). For example, female GABAergic neurons showed a total of 329 DEGs, of which only 48 were shared with other cell types, notably astrocytes (15) and oligodendrocytes (7) (Figure 2D). Similarly, male endothelial cells had a total of 261 DEGs, of which only 17 DEGs were in common with astrocytes and 5 with oligodendrocytes (Figure 2E). We confirmed the sex and stress specificity of our results by validating the change in expression of the top two DEGs in GABAergic neurons, the most responsive population across sexes. By RNAscope, we checked for the expression levels of *Gapdh* and *Ndn* selectively in GAD1$^+$ cells of the PVN and confirmed a reduction in their levels selectively in females (Figures 1B, 1C, and S3D). Interestingly, both genes have been implicated in the cellular response to stress.[27,28]

Because some cell types (such as astrocytes, oligodendrocytes, endothelial cells, ependymal cells, vasopressin neurons, and pericytes) were stress responsive in both sexes, we also explored their response overlap between sexes. A similarity index based on the DEGs overlap (Figure 2F, left column) showed that only the top three most responsive cell types, namely, astrocytes, oligodendrocytes, and endothelial cells, had any degree of similarity (Figure 2F, right). Collectively, our results demonstrate that exposure to an acute stressor elicits a transcriptional response in the PVN in several neuronal and non-neuronal cells, which is mostly unique to the cell type and differs substantially between sexes.

Chronic stress changes the cell-type-specific response to acute stress in a sex-dependent manner

Dysregulation of the HPA axis in connection with exposure to chronic stress often characterizes stress-related psychiatric disorders.[7] Having shown that ARS elicits transcriptional signatures that are cell type and sex specific, we next explored how these molecular signatures changed in mice that were exposed to chronic stress before ARS.

We exposed a second cohort of mice to unpredictable CMS before receiving the 15-min ARS (Figure 1A, CMS ARS). The CMS paradigm included a random combination of two psychophysical, social, or home-cage stressors per day for 21 days (see STAR Methods for the detailed list) and effectively caused anhedonia and depressive-like phenotype in the splash test, as measured in a separate cohort (Figures S1I–S1M). Compared with controls, CMS mice displayed the hallmark features of chronically stressed mice, including reduced body weight gain, coat deterioration, and enlarged adrenal glands (Figures S1N–S1Q). The differential gene expression analysis on CMS control and CMS ARS cells identified cell-type-specific molecular signatures associated with ARS after chronic stress exposure in both sexes. These molecular signatures differed from Baseline ARS both in the extent and involvement of cell types (Figure 3A). We then explored how each individual cell type was impacted by previous exposures to stress (CMS or baseline). We defined the stress response of each cell type by the "extent," i.e., the number of DEGs, and the "magnitude," i.e., the absolute median log fold change (logFC) of the response, and calculated the distance for each cluster between CMS and baseline (Figure S3E). We then calculated the sum of distances between males and females (Figure 3B) to establish which cell types were most affected by the stress history across sexes. Using this approach, we identified a range of susceptibility scores in which astrocytes, ependymal cells, and pericytes ranked the lowest, whereas endothelial cells, GABAergic neurons, and oligodendrocytes were mildly to prominently affected by the CMS history across sexes (Figure 3B). Interestingly, only female glutamatergic neurons showed a strong susceptibility (Figures S3F and S3G). In contrast, some of the top responders to ARS at baseline (Figure 2A), such as astrocytes, showed minimal influence by exposure to chronic stress (score −1.66; Figures S3F and S3H). We then focused on the top-ranking cells because their high susceptibility scores might indicate a differential involvement in the stress response across sexes. Oligodendrocytes were the top-ranking cell type with a calculated susceptibility score of 4.92, which was more than twice the score of the second ranked, the GABAergic neurons (score, 2.40). Overall, these results suggest that previous exposure to chronic stress influences the ability of different cell types, especially oligodendrocytes, to respond to an acute stressor.

Oligodendrocytes display stress responsivity modulated by sex and history of stress exposure

Our analysis suggests that the stress-induced transcriptional response of oligodendrocytes is sensitive to a history of chronic stress, a risk factor often associated to psychiatric disorders.[8] Because oligodendrocytes are dynamic glial cells now identified as active players in stress-related disorders,[29] we further explored any sex differences in their stress response.

In contrast with other cell types with low susceptibility scores (such as astrocytes; Figure S3H), the ARS response of oligodendrocytes showed limited overlap in DEGs between baseline and CMS backgrounds (Figure 3C). In addition, after CMS, ARS induced one-third of the DEGs found at baseline in females but 14 times more in males (Figure 3C). In females, 94 genes were differently expressed in oligodendrocytes after ARS at baseline, whereas only 27 were differentially expressed after ARS under CMS background. In addition, of these 27 DEGs, 70% of them (19 of 27) were dysregulated also in Baseline ARS, indicating that CMS largely blunted the ARS response in female mice (Figure 3C). However, in male mice, the opposite was true: 46 genes were differentially expressed after ARS at baseline, but 625 were changed after ARS with CMS exposure, indicating that CMS enhanced the ARS response in male cells. The male response to ARS with previous CMS mainly had DEGs (95%, 625 of 658) that were not dysregulated at baseline. Furthermore, these distinctions were even more prominent when taking into consideration directionality of the dysregulation. In females, the shared DEGs could often be found regulated in opposite directions with or without previous exposure to CMS, whereas in males, they often were dysregulated in the same direction (Figure 3D). This observation held true also at the larger scale of the transcriptome, suggesting a generalized trend. A rank-rank hypergeometric overlap (RRHO) analysis compares the change in expression of all genes at once between two conditions. As such, it allows to identify shared patterns of dysregulation, such as commonly upregulated genes (Figure 3D, top right and bottom left quadrants) or oppositely regulated genes (Figure 3D, top left and bottom right quadrants). We used an RRHO analysis to assess how similar the differential expression pattern induced by ARS was with or without a history of CMS. Overall, females showed a group of genes upregulated at baseline but downregulated in CMS (Figure 3E, top left quadrant). In contrast, genes upregulated at baseline in males were often upregulated in CMS background as well (Figure 3E, top right and bottom left quadrants). To better find key players in the differences observed in oligodendrocytes, we performed a hierarchical cluster analysis aimed at identifying groups of genes similarly regulated across conditions. Our analysis yielded 16 different gene clusters (Figures S3I–S3J; Table S4). Among these clusters, we found several interesting expression patterns. For example, clusters 4 and 16 summarized ARS response under baseline condition regardless of sex, but no cluster was found that represented

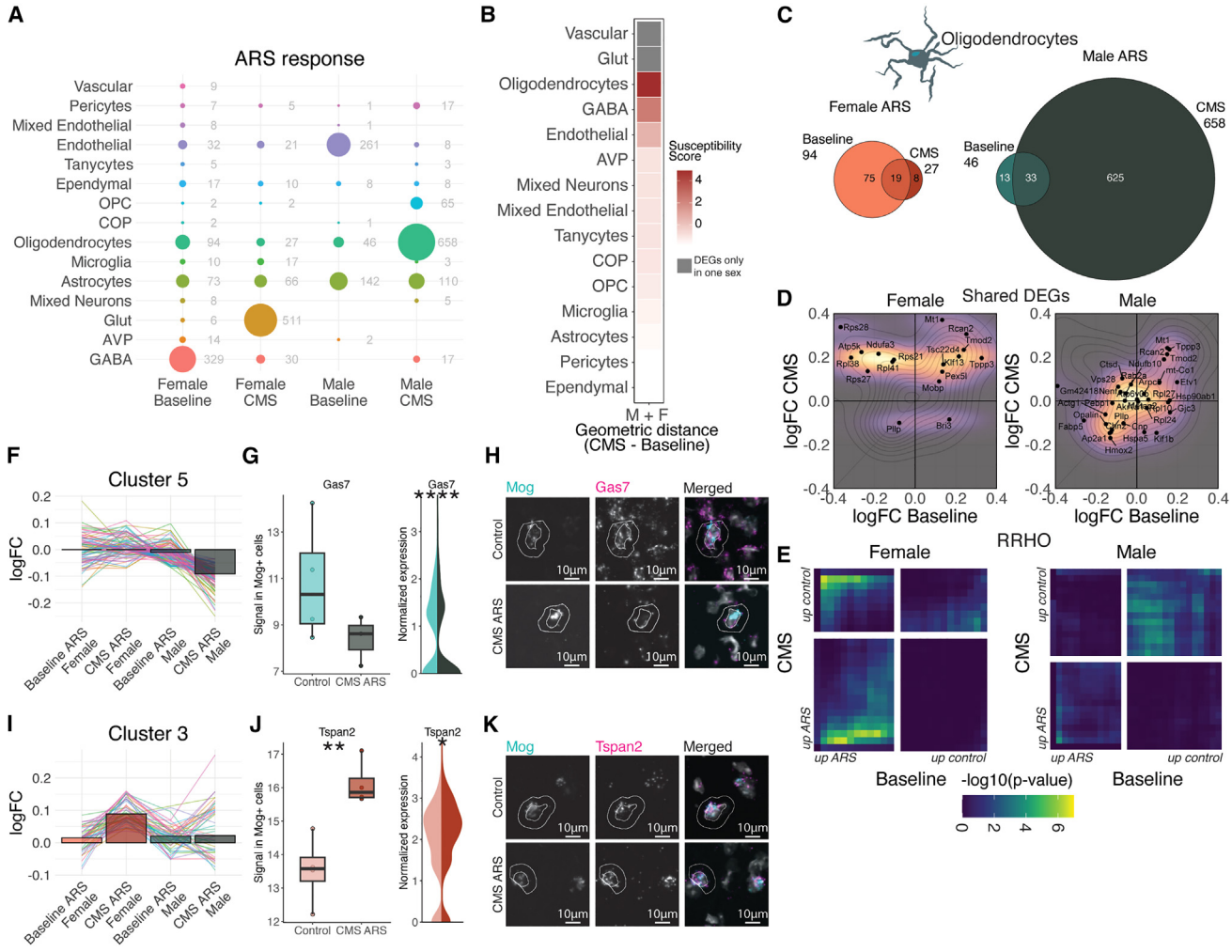

Figure 3. Oligodendrocytes' stress response is particularly susceptible to a history of chronic stress in a sex-specific way

(A) Dot plot of DEGs in the ARS response for baseline and CMS history in males and females.

(B) Heatmap plot of *Z*-scored Euclidean distances between baseline and CMS ARS response summed between sexes. Oligodendrocytes are the top susceptible cell type.

(C) Number of DEGs to ARS for oligodendrocytes showing an opposite trend between sexes.

(D) DEGs shared between backgrounds by their log fold change (logFC). Background colors show density distribution.

(E) Rank-rank hypergeometric overlap (RRHO) analysis for oligodendrocytes showing sex-specific patterns. Top right and bottom left quadrants represent genes concordantly dysregulated (down and up, respectively); top left and bottom right quadrants show genes dysregulated in opposite directions.

(F) Cluster 5 from hierarchical clustering of oligodendrocytes DEGs is representative of CMS ARS male response. Bars show the median logFC of each gene in the cluster.

(G) *Gas7* is the top DEG representing cluster 5. Expression levels (number of RNA puncta, boxplot) measured by RNAscope in oligodendrocytes (Mog^+ cells) compared with scRNA-seq results (violin plots). Despite a trend, statistical significance was not reached because of high spread in control animals (t test, Gas7: $t(1) = 2.30$, $p = 0.19$). Boxplots: interquartile range (IQR) and median; whiskers: minimum and maximum value ± 1.5 IQR.

(H) Representative RNAscope images for control and CMS ARS male samples (scale bars, 10 µm). Nucleus and cell ROIs for the example cell are shown in white.

(I) Cluster 3 from hierarchical clustering of oligodendrocytes DEGs is representative of CMS ARS female response. Bars show the median logFC of each gene in the cluster.

(J) *Tspan2* is the top DEG representing cluster 3. Increased expression levels (number of RNA puncta, boxplot) measured by RNAscope in oligodendrocytes (Mog^+ cells) compared with scRNA-seq results (violin plots) (t test, Tspan2: $t(1) = 17.27$, $p = 0.006$).

(K) Representative RNAscope images for control and CMS ARS female samples (scale bars, 10 µm). Nucleus and cell ROIs for the example cell are shown in white. Boxplots: interquartile range (IQR) and median; whiskers: minimum and maximum value ± 1.5 IQR.

See also Figure S3 and Table S4.

CMS ARS across sexes. Instead, cluster 5 and cluster 3 collected the male and female CMS ARS-specific response, respectively (Figures 3F and 3I). Cluster 5 was characterized by the downregulation of many genes associated to growth and proliferation processes, such as *Gas7*, *Pmp22*, *Cntn22*, *Vapa*, *Tspan15*, *Tspan3*, *Hspa5*, *Gjc2*, *Kif1b*, and *Kif1bp*,

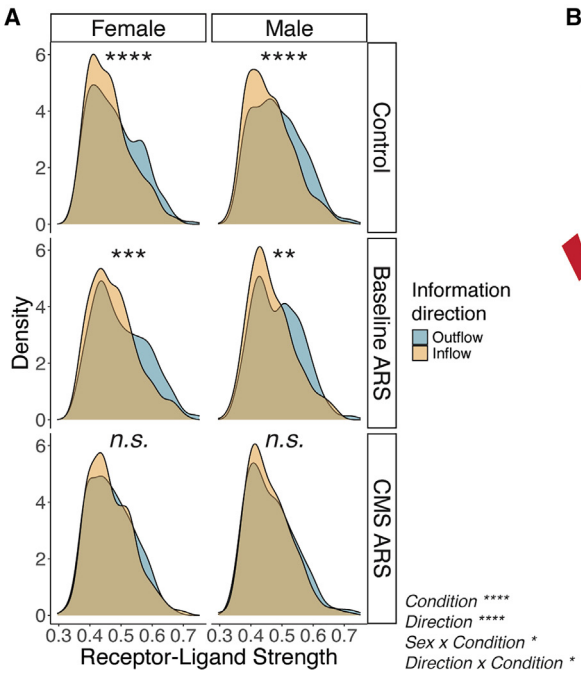

Figure 4. Interaction networks between oligodendrocytes and neurons

(A and B) Stress alters the balance between outgoing (oligodendrocyte ligand – neuronal receptor) and ingoing (neuronal ligand – oligodendrocyte receptor) interactions between oligodendrocytes and neurons. (A) Density plot of edge weights for receptor-ligand pairs per condition (Control includes both backgrounds collapsed). After CMS ARS, outflow pairs with high strength are selectively lost. Three-way ANOVA: condition, $F_{2,\ 4{,}961} = 15.39$, $p = 2.17 \times 10^{-7}$; direction, $F_{1,\ 4{,}961} = 56.79$, $p < 5.74 \times 10^{-14}$; sex × condition, $F_{2,\ 4{,}961} = 3.82$, $p = 0.022$; direction × condition $F_{2,\ 4{,}961} = 3.84$, $p = 0.022$, pairwise comparisons, Tukey's post hoc corrected: ****$p < 0.0001$, ***$p < 0.001$, **$p < 0.01$. (B) Scheme of the difference in oligodendrocyte-neuron interaction in the three conditions (Control, Baseline ARS, and CMS ARS).

n.s., not significant. See also Figure S4 and Table S5.

suggesting that the male-specific CMS ARS response might be arising by a changed maturation process. *Gas7*, the gene with the biggest logFC, for example, has been recently shown to be necessary for achieving oligodendrocyte maturation.[30] Cluster 3, in contrast, was mostly characterized by the upregulation of translation processes (*Rpl37*, *Slc38a2*) but also developmental processes (*Tspan2*, *Arpp19*). In particular, the top DEG for females, *Tspan2*, is known to regulate oligodendrogenesis,[31] possibly suggesting that similar but opposite processes are taking place in the two sexes. Thus, we used RNAscope to validate these top two genes in mature oligodendrocytes (marked by *Mog* expression) (Figures 3G, 3H, 3J, and 3K). Although we successfully validated the increase in *Tspan2* in female cells (Figures 3J and 3K), we observed reduction in *Gas7* levels to the expected extent that did not reach statistical significance, probably because of high variability in controls and reduced sample size (Figures 3G and 3H).

Overall, our data suggest that the transcriptional response to an acute stress of oligodendrocytes is influenced by CMS previous exposure, which differentially affects the sexes and possibly involves changes in oligodendrogenesis.

Stress alters the strength and balance of interaction networks between oligodendrocytes and neurons

Aside from generating the myelin sheath wrapped around neurons, oligodendrocytes contribute to maintaining regional homeostasis, sensing the change in the environment, and bidirectionally exchanging information with neurons for axonal maintenance and synaptic function.[32,33] Given the close interaction between oligodendrocytes and neurons, we investigated whether ARS exposure (with or without CMS) impacts the relationship between these two cell types. To address this question, we built cell-cell interaction networks to quantify ligand-receptor interactions as edge weights between oligodendrocytes and neurons. We further assessed which of the receptor-ligand pairs significantly (permutation analysis, $p < 0.05$) changed strength in response to ARS and found that several receptor-ligand pairs were altered by ARS exposure (Table S5). Because no major differences were observed between subpopulations of neurons, all pairs were aggregated into a single analysis (Figure S4A). Importantly, the identified dysregulated receptor-ligand pairs were of both possible direction types: pairs with a ligand in oligodendrocytes and a receptor in neurons (outflow) and pairs with a ligand in neurons and a receptor in oligodendrocytes (inflow) (Figure S4B). To understand whether stress exposure impacted preferentially either direction of communication, we looked at the distribution of strength of all altered receptor-ligand pairs in each state (Control, Baseline ARS, and CMS ARS) and compared the distribution of strength of each receptor-ligand pair based on their direction of communication (Figure 4A). We combined the two control conditions (Baseline Control and CMS Control) because they showed similar distributions (Figure S4C). In control conditions, the outflow of information from oligodendrocytes was stronger than the inflow. After ARS, this relationship still existed at baseline but was lost with the CMS history because of an overall decrease in ligand strength of the output direction (outflow). Our results suggest that the exposure to ARS after CMS preferentially weakens the output direction from oligodendrocytes to neurons in both sexes (Figure 4B).

Male oligodendrocytes in the PVN show an immature morphology after stress exposure

Because interactions between neurons and oligodendrocytes change along their developmental trajectory,[34] oligodendrocytes actively proliferate and mature throughout adulthood,[35] and we found DEGs possibly implicated in developmental processes, we hypothesized that stress exposure might affect the

development or morphology of oligodendrocytes in a sex-specific way. To explore this further, we performed a pseudotime trajectory analysis on all clusters belonging to the oligodendrocyte lineage (OPCs, COPs, and mature oligodendrocytes; Figures S5A and S5B). A pseudotime analysis uses gene expression data to infer the maturation state of each cell within a group, by determining the most and least mature cells and ordering the others along developmental branches. As such, for each cell we computed a pseudotime value ranging from 0 (immature) to 30 (mature), which successfully ordered cells from OPCs to COPs and to mature oligodendrocytes (Figures 5A and S5C). We then compared how cells distributed along this continuous value and whether stress caused any shift in pseudotime values occupancy. Comparing the pseudotime distribution of control and CMS ARS samples, we found that stressed male cells showed a significant shift toward more immature stages: 50% of all male cells were contained in a pseudotime interval 90% the size of the control one (approximately 1.6 points smaller interval; dotted lines, Figure 5B). In contrast, females did not show any significant differences, nor did any sexes after Baseline ARS (Figure S5D). During their development, oligodendrocytes activate several transcriptional programs,[36] among them Mog is upregulated in the final stages of maturations, whereas Olig2 gets downregulated. The mapping of these two genes along the pseudotime indeed confirmed this expected trend (Figure S5E, top). To explore whether the developmental trajectory of male oligodendrocytes could be impacted by stress, we stained for *Mog* and *Olig2* expression levels by RNAscope and verified whether their reciprocal expression levels were maintained even in stress conditions. Their quantification by RNAscope showed very similar trends to the one obtained by pseudotime analysis (Figure S5E, bottom) and confirmed the existence of $Mog^{-}/Olig2^{++}$, $Mog^{++}/Olig2^{++}$, and $Mog^{+}/Olig2^{+}$ cells and all combinations of intermediate expression. We did not observe differences in Olig2 expression levels in Mog^{+} cells in either sex (Figure S5F). In contrast, in males after CMS ARS, more $Olig2^{+}$ cells (younger cells) showed low to no Mog, supporting the idea that males have more immature cells than controls (Figure 5C). This was not true for female $Olig2^{+}$ cells (Figure S5G), consistent with the pseudotime results.

In their development, gray matter oligodendrocytes generate several branches and ramifications to contact surrounding cells;[35,37] thus, we then checked whether male oligodendrocytes with CMS history would show sex-specific less mature morphology. To characterize their morphology in the PVN, we used immunostaining of Tmem10, a specific marker for the cell body and the projections of mature oligodendrocytes[38] (Figures 5D and 5E) and confirmed their identity with Olig2, given its persistent expression across the developmental trajectory.[39] We then traced the cell morphology in controls and stressed mice with CMS history and explored the ramification structure of these cells using a Sholl analysis (Figures 5F and 5G). We did not observe any differences in soma size between sexes or condition (Figure S5H) but identified a significant interaction between sex and condition in branching. Cells from male mice with a CMS history appeared less complex with significantly less ramifications and shorter branches. The Sholl analysis also identified the existence of sex differences in the size of oligodendrocytes, with female oligodendrocyte having a maximal branching extension on average 5.6 μm wider (Figure S5I) (maximum radius: female control, 42.11 μm [±4.86]; stress, 38.20 μm [±3.94]; male control, 35.15 μm [±5.85]; stress, 33.91 μm [±5.69]). We also found a trend for smaller radius for cells under stress (control, 38.63 μm [±6.29]; stress, 36.06 μm [±5.17]) (Figure S5I). Our results suggest that a combination of chronic and acute stress affect the morphological state of the oligodendrocytes residing in the PVN in a sex-specific way.

DISCUSSION

Recent studies exploring stress-induced transcriptomic changes have suggested that differences between the sexes could result from different cell-type contributions in males and females.[16,19,20] However, these studies lacked single-cell resolution to directly address this question. Here, we used single-cell transcriptomics to explore adult sex differences to stress exposure and show that the PVN transcriptional response to acute stress substantially differs between cell types and sexes. Our findings suggest that previous stress exposure modulates this response in a sex- and cell-type-dependent way. Furthermore, we show that these differences impact on cell development and morphology *in vivo.* Finally, our study provides a rich resource for researchers and clinicians interested in exploring the important interplay between sex and stress.

Our unbiased sampling of a large number of individual cells (~35,000) across the entire PVN, with limited contamination from neighboring regions (Figure S2), identified all the major cell types previously reported in the PVN.[22,25,40,41] However, we extend this knowledge further by providing higher-resolution characterization of subpopulations and rare cell types, such as subtypes of microglia, ependymal cells, and tanycytes. Although it is difficult to directly compare our cell annotations with previously published datasets because of methodological differences, total number of cells, and their high heterogeneity,[18,23,42–44] we identified several of the major hypothalamic neuropeptides, such as *Avp*, *Oxt*, *Trh*, *Calbn2*, *Th*, *Gal*, and *Tac1*, which others have found as well.[42,45] Cells expressing the hallmark peptide of PVN, Crh, clustered together within a specialized glutamatergic subcluster that also expresses Trh. The co-localization of these markers indicates that the absence of pure Crh clusters was mostly due to limited resolution, because Crh and Trh are predominantly expressed in glutamatergic neurons, particularly within the same parvocellular cells.[46,47]

Most importantly, our dataset identified extensive sex differences in both neuronal and non-neuronal stress-responsive cells. We show that more cell types are responsive to an acute stressor in females and that a history of chronic stress changes this response in a sex-specific way. Like other datasets, glial cells were the biggest source of DEGs for males.[22,48] For example, endothelial cells had the highest number of DEGs after acute restraint in the dataset presented here, but also after chronic social defeat.[22] In contrast, DEGs after ARS in females were mostly derived from neuronal populations. Because DEGs in male GABAergic neurons were elicited only by chronic social defeat[22] or with the combination of CMS ARS in this

CellPress
OPEN ACCESS

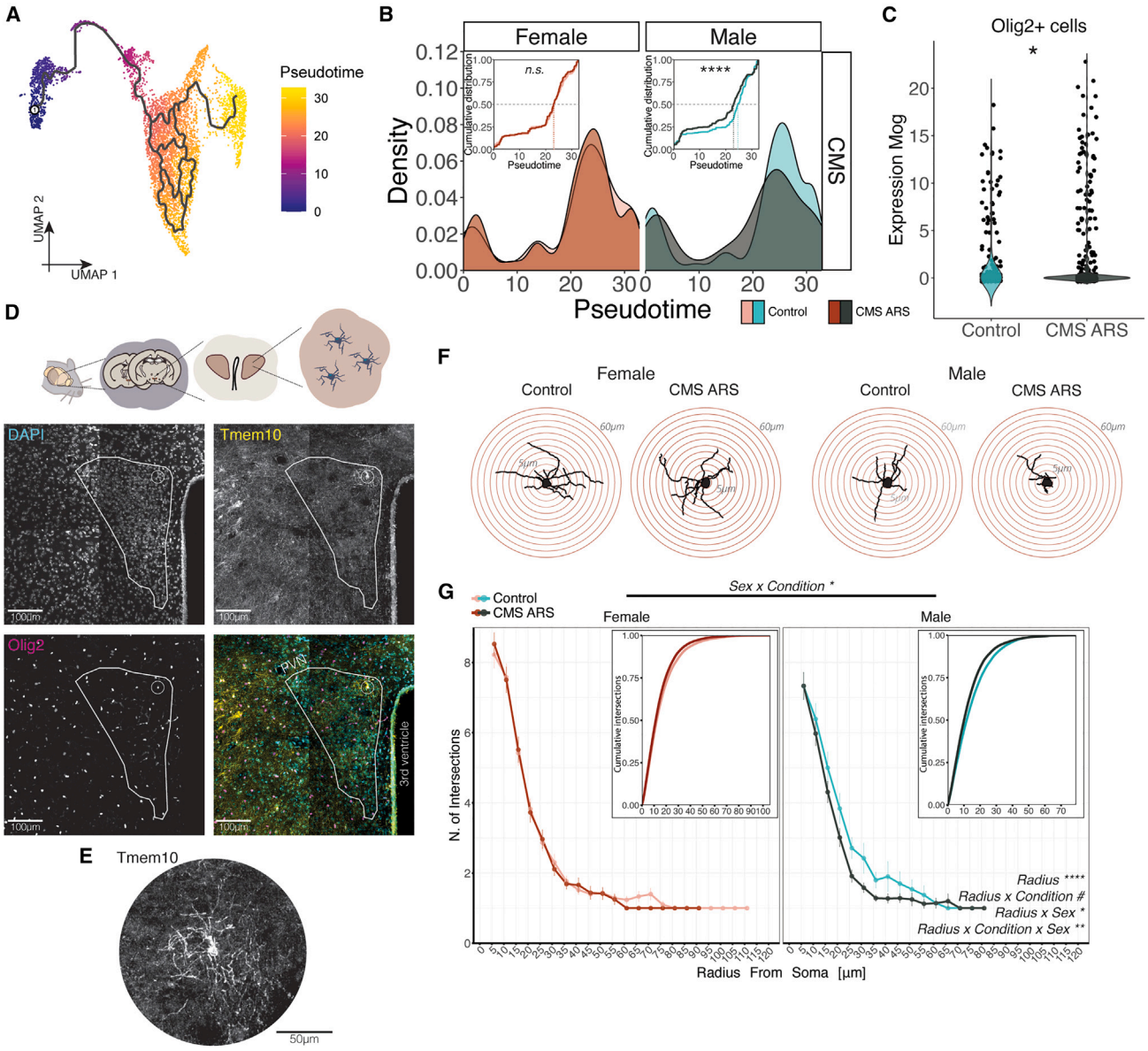

Figure 5. Stress impacts on oligodendrocytes state

(A and B) Pseudotime analysis reveals a shift toward immature stages in male oligodendrocytes with CMS history. (A) UMAP plot of pseudotime analysis. Pseudotime root is circled. (B) Density plot of cells across pseudotime. Inset plots show cumulative distributions (two-sided Kolmogorov-Smirnov test; female, $D = 0.059$, $p = 0.182$; male, $D = 0.168$, $p = 2.197 \times 10^{-6}$).

(C) RNAscope showed more *Olig2*$^{+}$ cells with low or absent *Mog* expression in males after CMS ARS ($N_{control} = 41$, $N_{CMS\ ARS} = 66$, Wilcoxon rank-sum test, $F(1) = 40{,}141.5$, $p = 0.04$).

(D) Representative images of oligodendrocytes traced in the PVN (scale bars, 100 µm).

(E) Example of Tmem10 signal used for tracing (scale bar, 50 µm).

(F) Representative skeletons of female (left) and male (right) oligodendrocytes.

(G) Sholl analysis on branching of female (left) and male (right) oligodendrocytes shows a sex × condition effect on cell morphology (linear nested mixed-effect model, radius, $F = 2746.833$, $p < 2.2 \times 10^{-16}$; radius × condition, $F = 3.741$, $p = 0.053$, radius × sex, $F = 10.153$, $p = 0.0015$, condition × sex, $F = 6.305$, $p = 0.0177$, radius × condition × sex, $F = 9.391$, $p = 0.0022$). Sholl plots showing the number of intersections per distance from the radius. Inset plots show cumulative distribution of intersections. ****$p < 0.0001$, ***$p < 0.001$, **$p < 0.01$, *$p < 0.05$, $^{\#}p < 0.1$. Number animals per condition and sex = 6, number of traced cells: F CMS = 97, F ctrl = 82, M CMS = 81, M ctrl = 64. Data shown as mean ± SD.

n.s., not significant. See also Figure S5.

dataset, female GABAergic neurons may exhibit heightened responsiveness and greater sensitivity to stress compared with males. These female GABAergic neurons display a high number of DEGs, including steroid hormone chaperones (e.g., *Hsp90aa1*, *Hsp90ab1*, and *Dnaja1*), genes associated to synaptic release (e.g., *Snap47*, *Nrnx1*, *Nrnx3*, *Rab3a*, and *Syt1*), and GABA cycle genes (*Slc32a1*, *Slc6a1*, *Gabrb1*, and *Gabrb2*). These DEGs suggest that GABAergic neurons may respond to stress-dependent increased circulating steroid hormones and regulate cell activity in a distinct manner from males. A similar sex-specific transcriptional response to stress of GABAergic neurons has been observed also in other brain regions, such as the prefrontal cortex.[49] The nearly exclusive presence of neuronal DEGs following ARS in females implies the existence of distinct cellular sensitivities to stress. Previous studies have linked the functionality of GABAergic neurons to the regulation of PVN activity,[50] although the hyperresponsiveness of the female HPA axis to acute challenges is extensively documented.[4,11] Our results provide a possible molecular link between these two processes. Notably, in both MDD patients and mouse stress models, diverse molecular mechanisms can lead to similar pathological outcomes.[15,20] Similarly, this sex-specific neuronal response might suggest that stress processing at the cellular level is dimorphic, despite ultimately manifesting with similar characteristics.

Curiously, the combination of chronic and acute stress exposed an interesting pattern of activation and sensitivity to the background within the female GABAergic-glutamatergic circuitry. Under baseline conditions, GABAergic cells respond the strongest in females. However, with a history of CMS, these cells lose a significant portion of response. In contrast, glutamatergic cells increase their response under CMS conditions. Alterations in the balance between glutamate and GABA are of particular importance due to their association to many psychiatric conditions.[51,52] Our results further suggest that sex might enhance or attenuate the system balance in response to stress, which is in accordance with previous work conducted in the cortex.[53] The GABA-glutamate system is an important target for antidepressants,[53] and both classic and rapid antidepressants, such as ketamine, have been shown to act in a sex-specific way.[54] Future studies could provide insights into how sex influences the GABA-glutamate system, which may lead to new and more effective drugs designed to target men or women specifically.

Finally, we showed the relevance of this dataset by identifying the oligodendrocytes as the cell type most affected by a history of CMS and by providing their in-depth characterization. Although recent studies have described how oligodendrocytes are sexually dimorphic cells in terms of morphology, proliferation, and survival,[55–58] to the best of our knowledge, sex differences in stress reactivity have not been identified before. Our data show that male, but not female, oligodendrocytes are strongly affected by exposure to CMS. This exposure modulates their transcriptomic response to stress, changes their interaction with surrounding neurons, and determines a morphological alteration possibly caused by altered maturation state. Accordingly, recent findings identified a change in interaction between neurons and oligodendrocyte progenitors in postmortem brains of male MDD patients,[59] and an aberrant proliferation and differentiation of OPC followed by demyelination was observed in chronically defeated male mice.[60,61] The shift in pseudotime we observed could be explained by a similar mechanism involving changes in OPC proliferation and maturation during challenges to brain homeostasis. The change in Mog levels in Olig2^{+} (younger) cells we describe supports this hypothesis. In addition, our results suggest that these alterations described in male-only studies might be sex specific, complementing recent transcriptomic findings that propose an opposite effect of MDD in male and female oligodendrocytes.[20] Although we still do not fully understand why male and female cells show a different sensitivity to stress, elevated corticosterone levels, a hallmark of stress exposure, modulate proliferation and maturation of oligodendrocytes.[62] We propose exploring the effect of sex on corticosterone sensitivity in oligodendrocytes and further explore proliferation or resilience to cell death under stress in future investigations. Oligodendrocytes and neuronal interactions have also not been explored in the context of sex differences. Although our bioinformatics analysis might suggest that stress preferentially alters the outflow of information from oligodendrocytes to neurons, it does not exclude the possibility that oligodendrocytes might be acting as sentinels for an underlining sexually different neuronal circuitry and its changes to stress. Our dataset can serve as a valuable resource for researchers interested in further exploring the transcriptional alterations in the subtypes of neurons and in oligodendrocytes. Future studies in these directions have the potential to identify new candidate genes that regulate oligodendrocyte survival and oligodendrocyte-neuronal communication. In addition, such studies could also identify valuable new drug targets for the treatment of stress-related psychiatric disorders[29] and other disorders with pronounced sex bias in the involvement of oligodendrocytes, such as multiple sclerosis.[63]

Limitations of the study

Although this study provides important insights, there are some limitations that should be addressed. First, in order to be able to perform timed stress paradigms, we were not able to behaviorally validate CMS in the animals that were used for scRNA-seq but relied on physical parameters for its efficacy. However, we showed that the CMS paradigm is effective in causing a depressive-like phenotype in the splash test, as well as in physical aspects (Figures S1I–S1M). In addition, in our dataset we observe only a small (∼15%) but significant increase in adrenal size, which seems minimal when compared with other paradigms. However, CMS is specifically designed to apply a mild stress load on the individual, resembling a more naturalistic setup,[64] and it is not uncommon to not observe differences in adrenal weight following CMS.[65–67] Second, given our goal to compare both sexes in a selective but small brain region (PVN) and in order to obtain the right number of cells to generate a healthy single-cell suspension and generate high-quality single-cell data, we had to pool multiple animals (n = 5) per one technical sample. Although this means we do not have both technical and full biological replicates in our dataset, having pooled multiple animals we expect to maintain at least partial biological variability within samples, something that has been shown for other sequencing approaches.[68] In addition, we chose to use scRNA-seq rather

than single nuclei, which does not allow for the unbiased interpretation of immediate-early genes (IEGs), which can be activated by the dissociation process. To minimize this effect and maximize the viability and reliability of our data, we took several precautions. We generated and maintained cell suspensions in cold and oxygenated cerebrospinal fluid (CSF), minimized processing time, and avoided the use of transcription inhibitors that could be toxic. Furthermore, samples were collected at a time point (5 h) to avoid any potential IEG response to stress. Previous studies have demonstrated the robustness of protocols like ours and the relevance of this second wave of transcription when analyzing the stress response.[18,22,24,44,69–72]

Finally, our data represent important insights on the role of the PVN in the stress response and in particular of oligodendrocytes in this region. Because oligodendrocytes are widespread in the brain, it could be reasonable to think that a similar response might be found also in other gray matter regions. Although we could not validate our results in every other relevant region, it is interesting to point out that stress elicited by the forced swim test led to changes in oligodendrocytes from the hippocampus, which are consistent with our findings in the PVN[48] residing in other brain areas.

Conclusions

Previous scRNA-seq datasets with male and female hypothalamic samples have mostly focused on anatomical characterization of broad hypothalamic regions[17,23] or selectively neuronal populations.[18,23] Only a few have studied the effects of stress in males and females, typically limited to single stress manipulations[44] and broader hypothalamic regions.[23] In contrast, our unbiased dataset covers neuronal, glial, and stromal cell types of selectively the PVN, a highly relevant region for stress, allowing the exploration of multiple stress combinations in neuronal and non-neuronal populations of adult male and female mice. Altogether, our results indicate the need for more single-cell resolution studies in females and males and highlight directions to dissect the molecular processes driving sex differences in normal physiology and in response to stress. When combined with other recent studies,[17,18] our results provide further molecular and cellular characterization of the hypothalamus and identify several cell types as priorities in which to explore sex differences in the context of stress. Investigation into how many of these differences exist in the human brain could provide new understanding of the origin of the sex differences in brain structure and function.[73]

Researchers interested in dissecting stress-related disorders will be able to use the online platform we provide (available at https://male-female-stress.weizmann.ac.il/shinyApp/) to study the role of sex on the HPA axis at single-cell resolution, which might generate cell targets for sex-specific treatment of stress-related psychiatric disorders.

STAR★METHODS

Detailed methods are provided in the online version of this paper and include the following:

- KEY RESOURCES TABLE
- RESOURCE AVAILABILITY
  - Lead contact
  - Materials availability
  - Data and code availability
- EXPERIMENTAL MODEL AND SUBJECT DETAILS
  - Mice husbandry
- METHOD DETAILS
  - Stressors
  - Splash test (ST)
  - Corticosterone assessment
  - Single cell RNA-sequencing
  - RNAscope
  - Morphology analysis of oligodendrocytes
- QUANTIFICATION AND STATISTICAL ANALYSIS
- ADDITIONAL RESOURCES
  - Web app

SUPPLEMENTAL INFORMATION

Supplemental information can be found online at https://doi.org/10.1016/j.celrep.2023.112874.

ACKNOWLEDGMENTS

We thank Prof. Dr. Elior Peles and Dr. Nimrod Elazar (Weizmann Institute of Science) for providing the antibody anti-Tmem10; the staff from the animal facility at the Max Planck Institute of Psychiatry for help with animal care; the technical staff from the Max Planck Institute of Psychiatry, especially Daniela Harbich, Bianca Schmid, Laura Poehlenz, and Stefanie Unkmeir, for the technical support; Lior Michael (Weizmann IT team) and Lior Segev (Weizmann Institute of Science) for app hosting and deployment; Liat Alyagor and Roni Oren for the support with RNAscope; and Jessica Keverne for writing support and advice. J.P.L. holds fellowships from the European Molecular Biology Organization (EMBO-ALTF 650-2016), Alexander von Humboldt Foundation, and Canadian Biomarker Integration Network in Depression (CAN-BIND). A.C. is the incumbent of the Schwartz Family Professorial Chair in Neurobiology at WIS and the head of the MPS-WIS Laboratory for Experimental Neuropsychiatry and Behavioral Neurogenetics. A.C. has received research support from the Ruhman Family Laboratory for Research in the Neurobiology of Stress, Bruno and Simone Licht, the Perlman Family Foundation, the Adelis Foundation, and Sonia T. Marschak.

AUTHOR CONTRIBUTIONS

Conceptualization: E.B., J.P.L., and A.C.; software: E.B., A.F.U., and S.K.; formal analysis: E.B., S.K., A.F.U., and G.S.; investigation: E.B., J.P.L., A.R., A.K., R.S., and D.H.; writing – original draft: E.B.; writing – review & editing: E.B., A.K., A.F.U., S.K., M.V.S., J.P.L., and A.C.; supervision: J.P.L., A.C., and M.V.S.; funding acquisition: A.C.

DECLARATION OF INTERESTS

The authors declare no competing interests.

Received: June 23, 2022
Revised: May 19, 2023
Accepted: July 11, 2023
Published: July 29, 2023

REFERENCES

1. GBD 2016 Disease and Injury Incidence and Prevalence Collaborators; Vos, T., Abajobir, A.A., Abbafati, C., Abbas, K.M., Abate, K.H., Abd-Allah, F., Abdulle, A.M., Abebo, T.A., Abera, S.F., Aboyans, V., et al. (2017).

Global, regional, and national incidence, prevalence, and years lived with disability for 328 diseases and injuries for 195 countries, 1990-2016: A systematic analysis for the Global Burden of Disease Study 2016. Lancet *390*, 1211–1259. https://doi.org/10.1016/S0140-6736(17)32154-2.

2. Wittchen, H.U., Jacobi, F., Rehm, J., Gustavsson, A., Svensson, M., Jönsson, B., Olesen, J., Allgulander, C., Alonso, J., Faravelli, C., et al. (2011). The size and burden of mental disorders and other disorders of the brain in Europe 2010. Eur. Neuropsychopharmacol *21*, 655–679. https://doi.org/10.1016/j.euroneuro.2011.07.018.
3. McCarthy, M.M. (2016). Multifaceted origins of sex differences in the brain. Philos. Trans. R. Soc. Lond. B Biol. Sci. *371*, 20150106. https://doi.org/10.1098/rstb.2015.0106.
4. Heck, A.L., and Handa, R.J. (2019). Sex differences in the hypothalamic–pituitary–adrenal axis' response to stress: an important role for gonadal hormones. Neuropsychopharmacology *44*, 45–58. https://doi.org/10.1038/s41386-018-0167-9.
5. Krishnan, V., and Nestler, E.J. (2008). The molecular neurobiology of depression. Nature *455*, 894–902. https://doi.org/10.1038/nature07455.
6. Simmons, J.M., Winsky, L., Zehr, J.L., and Gordon, J.A. (2021). Priorities in stress research: a view from the U.S. National Institute of Mental Health. Stress *24*, 123–129. https://doi.org/10.1080/10253890.2020.1781084.
7. McEwen, B.S. (1998). Protective and Damaging Effects of Stress Mediators. N. Engl. J. Med. *338*, 171–179. https://doi.org/10.1056/NEJM199801153380307.
8. Van Praag, H.M. (2004). Can stress cause depression? Prog. Neuro-Psychopharmacol. Biol. Psychiatry *28*, 891–907. https://doi.org/10.1016/j.pnpbp.2004.05.031.
9. Di Segni, M., Andolina, D., and Ventura, R. (2018). Long-term effects of early environment on the brain: Lesson from rodent models. Semin. Cell Dev. Biol. *77*, 81–92. https://doi.org/10.1016/j.semcdb.2017.09.039.
10. Bangasser, D.A., and Valentino, R.J. (2014). Sex differences in stress-related psychiatric disorders: Neurobiological perspectives. Front. Neuroendocrinol. *35*, 303–319. https://doi.org/10.1016/j.yfrne.2014.03.008.
11. Goel, N., Workman, J.L., Lee, T.T., Innala, L., and Viau, V. (2014). Sex differences in the HPA axis. Compr. Physiol. *4*, 1121–1155. https://doi.org/10.1002/cphy.c130054.
12. Bangasser, D.A., and Cuarenta, A. (2021). Sex differences in anxiety and depression: circuits and mechanisms. Nat. Rev. Neurosci. *22*, 674–684. https://doi.org/10.1038/s41583-021-00513-0.
13. Bangasser, D.A., and Wicks, B. (2017). Sex-specific mechanisms for responding to stress. J. Neurosci. Res. *95*, 75–82. https://doi.org/10.1002/jnr.23812.
14. Brivio, E., Lopez, J.P., and Chen, A. (2020). Sex differences: Transcriptional signatures of stress exposure in male and female brains. Genes Brain Behav. *19*, e12643. https://doi.org/10.1111/gbb.12643.
15. Labonté, B., Engmann, O., Purushothaman, I., Menard, C., Wang, J., Tan, C., Scarpa, J.R., Moy, G., Loh, Y.H.E., Cahill, M., et al. (2017). Sex-specific transcriptional signatures in human depression. Nat. Med. *23*, 1102–1111. https://doi.org/10.1038/nm.4386.
16. Gegenhuber, B., and Tollkuhn, J. (2020). Signatures of sex: Sex differences in gene expression in the vertebrate brain. WIREs Dev. Biol. *9*, e348. https://doi.org/10.1002/wdev.348.
17. Moffitt, J.R., Bambah-Mukku, D., Eichhorn, S.W., Vaughn, E., Shekhar, K., Perez, J.D., Rubinstein, N.D., Hao, J., Regev, A., Dulac, C., and Zhuang, X. (2018). Molecular, spatial, and functional single-cell profiling of the hypothalamic preoptic region. Science *362*, eaau5324. https://doi.org/10.1126/science.aau5324.
18. Mickelsen, L.E., Bolisetty, M., Chimileski, B.R., Fujita, A., Beltrami, E.J., Costanzo, J.T., Naparstek, J.R., Robson, P., and Jackson, A.C. (2019). Single-cell transcriptomic analysis of the lateral hypothalamic area reveals molecularly distinct populations of inhibitory and excitatory neurons. Nat. Neurosci. *22*, 642–656. https://doi.org/10.1038/s41593-019-0349-8.
19. Gerhard, D.M., and Duman, R.S. (2018). Sex-Specific Molecular Changes in Depression. Biol. Psychiatry *84*, 2–4. https://doi.org/10.1016/j.biopsych.2018.05.005.
20. Seney, M.L., Huo, Z., Cahill, K., French, L., Puralewski, R., Zhang, J., Logan, R.W., Tseng, G., Lewis, D.A., and Sibille, E. (2018). Opposite Molecular Signatures of Depression in Men and Women. Biol. Psychiatry *84*, 18–27. https://doi.org/10.1016/j.biopsych.2018.01.017.
21. Nair, B.B., Khant Aung, Z., Porteous, R., Prescott, M., Glendining, K.A., Jenkins, D.E., Augustine, R.A., Silva, M.S.B., Yip, S.H., Bouwer, G.T., et al. (2021). Impact of chronic variable stress on neuroendocrine hypothalamus and pituitary in male and female C57BL/6J mice. J. Neuroendocrinol. *33*, e12972. https://doi.org/10.1111/jne.12972.
22. Lopez, J.P., Brivio, E., Santambrogio, A., De Donno, C., Kos, A., Peters, M., Rost, N., Czamara, D., Brückl, T.M., Roeh, S., et al. (2021). Single-cell molecular profiling of all three components of the HPA axis reveals adrenal ABCB1 as a regulator of stress adaptation. Sci. Adv. *7*, eabe4497. https://doi.org/10.1126/sciadv.abe4497.
23. Romanov, R.A., Zeisel, A., Bakker, J., Girach, F., Hellysaz, A., Tomer, R., Alpár, A., Mulder, J., Clotman, F., Keimpema, E., et al. (2017). Molecular interrogation of hypothalamic organization reveals distinct dopamine neuronal subtypes. Nat. Neurosci. *20*, 176–188. https://doi.org/10.1038/nn.4462.
24. Chen, R., Wu, X., Jiang, L., and Zhang, Y. (2017). Single-Cell RNA-Seq Reveals Hypothalamic Cell Diversity. Cell Rep. *18*, 3227–3241. https://doi.org/10.1016/j.celrep.2017.03.004.
25. Hajdarovic, K.H., Yu, D., Hassell, L.A., Evans, S., Packer, S., Neretti, N., and Webb, A.E. (2022). Single-cell analysis of the aging female mouse hypothalamus. Nat. Aging *2*, 662–678. https://doi.org/10.1038/s43587-022-00246-4.
26. Oakley, R.H., and Cidlowski, J.A. (2013). The biology of the glucocorticoid receptor: New signaling mechanisms in health and disease. J. Allergy Clin. Immunol. *132*, 1033–1044. https://doi.org/10.1016/j.jaci.2013.09.007.
27. Yoshikawa, K. (2021). Necdin: A purposive integrator of molecular interaction networks for mammalian neuron vitality. Gene Cell. *26*, 641–683. https://doi.org/10.1111/gtc.12884.
28. Nicholls, C., Li, H., and Liu, J.-P. (2012). GAPDH: A common enzyme with uncommon functions. Clin. Exp. Pharmacol. Physiol. *39*, 674–679. https://doi.org/10.1111/j.1440-1681.2011.05599.x.
29. Boda, E. (2021). Myelin and oligodendrocyte lineage cell dysfunctions: New players in the etiology and treatment of depression and stress-related disorders. Eur. J. Neurosci. *53*, 281–297. https://doi.org/10.1111/ejn.14621.
30. Marangon, D., Boda, E., Parolisi, R., Negri, C., Giorgi, C., Montarolo, F., Perga, S., Bertolotto, A., Buffo, A., Abbracchio, M.P., and Lecca, D. (2020). In vivo silencing of miR-125a-3p promotes myelin repair in models of white matter demyelination. Glia *68*, 2001–2014. https://doi.org/10.1002/glia.23819.
31. Yaseen, I.H., Monk, P.N., and Partridge, L.J. (2017). Tspan2: A tetraspanin protein involved in oligodendrogenesis and cancer metastasis. Biochem. Soc. Trans. *45*, 465–475. https://doi.org/10.1042/BST20160022.
32. Pepper, R.E., Pitman, K.A., Cullen, C.L., and Young, K.M. (2018). How do cells of the oligodendrocyte lineage affect neuronal circuits to influence motor function, memory and mood? Front. Cell. Neurosci. *12*, 399. https://doi.org/10.3389/fncel.2018.00399.
33. Habermacher, C., Angulo, M.C., and Benamer, N. (2019). Glutamate versus GABA in neuron–oligodendroglia communication. Glia *67*, 2092–2106. https://doi.org/10.1002/glia.23618.
34. De Biase, L.M., Nishiyama, A., and Bergles, D.E. (2010). Excitability and synaptic communication within the oligodendrocyte lineage. J. Neurosci. *30*, 3600–3611. https://doi.org/10.1523/JNEUROSCI.6000-09.2010.

35. Young, K.M., Psachoulia, K., Tripathi, R.B., Dunn, S.J., Cossell, L., Attwell, D., Tohyama, K., and Richardson, W.D. (2013). Oligodendrocyte dynamics in the healthy adult CNS: Evidence for myelin remodeling. Neuron *77*, 873–885. https://doi.org/10.1016/j.neuron.2013.01.006.

36. Kuhn, S., Gritti, L., Crooks, D., and Dombrowski, Y. (2019). Oligodendrocytes in Development, Myelin Generation and Beyond. Cells *8*, 1424. https://doi.org/10.3390/cells8111424.

37. Nave, K.A. (2010). Myelination and support of axonal integrity by glia. Nature *468*, 244–252. https://doi.org/10.1038/nature09614.

38. Golan, N., Adamsky, K., Kartvelishvily, E., Brockschnieder, D., Möbius, W., Spiegel, I., Roth, A.D., Thomson, C.E., Rechavi, G., and Peles, E. (2008). Identification of Tmem10/Opalin as an oligodendrocyte enriched gene using expression profiling combined with genetic cell ablation. Glia *56*, 1176–1186. https://doi.org/10.1002/glia.20688.

39. Wegner, M. (2001). Expression of transcription factors during oligodendroglial development. Microsc. Res. Tech. *52*, 746–752. https://doi.org/10.1002/jemt.1059.

40. Häusl, A.S., Hartmann, J., Pöhlmann, M.L., Brix, L.M., Lopez, J.-P.P., Brivio, E., Engelhardt, C., Roeh, S., Rudolph, L., Stoffel, R., et al. (2019). The co-chaperone Fkbp5 shapes the acute stress response in the paraventricular nucleus of the hypothalamus. Preprint at bioRxiv. https://doi.org/10.1101/824664.

41. Steuernagel, L., Lam, B.Y.H., Klemm, P., Dowsett, G.K.C., Bauder, C.A., Tadross, J.A., Hitschfeld, T.S., del Rio Martin, A., Chen, W., de Solis, A.J., et al. (2022). HypoMap—a unified single-cell gene expression atlas of the murine hypothalamus. Nat. Metab. *4*, 1402–1419. https://doi.org/10.1038/s42255-022-00657-y.

42. Romanov, R.A., Tretiakov, E.O., Kastriti, M.E., Zupancic, M., Häring, M., Korchynska, S., Popadin, K., Benevento, M., Rebernik, P., Lallemend, F., et al. (2020). Molecular design of hypothalamus development. Nature *582*, 246–252. https://doi.org/10.1038/s41586-020-2266-0.

43. Zeisel, A., Hochgerner, H., Lönnerberg, P., Johnsson, A., Memic, F., van der Zwan, J., Häring, M., Braun, E., Borm, L.E., La Manno, G., et al. (2018). Molecular Architecture of the Mouse Nervous System. Cell *174*, 999–1014.e22. https://doi.org/10.1016/j.cell.2018.06.021.

44. Campbell, J.N., Macosko, E.Z., Fenselau, H., Pers, T.H., Lyubetskaya, A., Tenen, D., Goldman, M., Verstegen, A.M.J., Resch, J.M., McCarroll, S.A., et al. (2017). A molecular census of arcuate hypothalamus and median eminence cell types. Nat. Neurosci. *20*, 484–496. https://doi.org/10.1038/nn.4495.

45. Kim, D.W., Washington, P.W., Wang, Z.Q., Lin, S.H., Sun, C., Ismail, B.T., Wang, H., Jiang, L., and Blackshaw, S. (2020). The cellular and molecular landscape of hypothalamic patterning and differentiation from embryonic to late postnatal development. Nat. Commun. *11*, 4360. https://doi.org/10.1038/s41467-020-18231-z.

46. Short, A.K., Thai, C.W., Chen, Y., Kamei, N., Pham, A.L., Birnie, M.T., Bolton, J.L., Mortazavi, A., and Baram, T.Z. (2023). Single-Cell Transcriptional Changes in Hypothalamic Corticotropin-Releasing Factor–Expressing Neurons After Early-Life Adversity Inform Enduring Alterations in Vulnerabilities to Stress. Biol. Psychiatry Glob. Open Sci. *3*, 99–109. https://doi.org/10.1016/j.bpsgos.2021.12.006.

47. Romanov, R.A., and Harkany, T. (2022). Neuronal heterogeneity in the paraventricular nucleus of the hypothalamus as revealed by single-cell RNA-seq. Curr. Opin. Endocr. Metab. Res. *25*, 100366. https://doi.org/10.1016/j.coemr.2022.100366.

48. von Ziegler, L.M., Floriou-Servou, A., Waag, R., Das Gupta, R.R., Sturman, O., Gapp, K., Maat, C.A., Kockmann, T., Lin, H.Y., Duss, S.N., et al. (2022). Multiomic profiling of the acute stress response in the mouse hippocampus. Nat. Commun. *13*, 1824. https://doi.org/10.1038/s41467-022-29367-5.

49. Girgenti, M.J., Wohleb, E.S., Mehta, S., Ghosal, S., Fogaca, M.V., and Duman, R.S. (2019). Prefrontal cortex interneurons display dynamic sex-specific stress-induced transcriptomes. Transl. Psychiatry *9*, 292. https://doi.org/10.1038/s41398-019-0642-z.

50. Decavel, C., and Van Den Pol, A.N. (1990). GABA: A dominant neurotransmitter in the hypothalamus. J. Comp. Neurol. *302*, 1019–1037. https://doi.org/10.1002/cne.903020423.

51. Marín, O. (2012). Interneuron dysfunction in psychiatric disorders. Nat. Rev. Neurosci. *13*, 107–120. https://doi.org/10.1038/nrn3155.

52. Prévot, T., and Sibille, E. (2021). Altered GABA-mediated information processing and cognitive dysfunctions in depression and other brain disorders. Mol. Psychiatry *26*, 151–167. https://doi.org/10.1038/s41380-020-0727-3.

53. Duman, R.S., Sanacora, G., and Krystal, J.H. (2019). Altered neurotransmitter deficits and reversal by novel treatments. Neuron *102*, 75–90. https://doi.org/10.1016/j.neuron.2019.03.013.Altered.

54. Chen, B.K., Luna, V.M., LaGamma, C.T., Xu, X., Deng, S.-X., Suckow, R.F., Cooper, T.B., Shah, A., Brachman, R.A., Mendez-David, I., et al. (2020). Sex-specific neurobiological actions of prophylactic (R,S)-ketamine, (2R,6R)-hydroxynorketamine, and (2S,6S)-hydroxynorketamine. Neuropsychopharmacology *45*, 1545–1556. https://doi.org/10.1038/s41386-020-0714-z.

55. Yasuda, K., Maki, T., Kinoshita, H., Kaji, S., Toyokawa, M., Nishigori, R., Kinoshita, Y., Ono, Y., Kinoshita, A., and Takahashi, R. (2020). Sex-specific differences in transcriptomic profiles and cellular characteristics of oligodendrocyte precursor cells. Stem Cell Res. *46*, 101866. https://doi.org/10.1016/j.scr.2020.101866.

56. Cerghet, M., Skoff, R.P., Bessert, D., Zhang, Z., Mullins, C., and Ghandour, M.S. (2006). Proliferation and death of oligodendrocytes and myelin proteins are differentially regulated in male and female rodents. J. Neurosci. *26*, 1439–1447. https://doi.org/10.1523/JNEUROSCI.2219-05.2006.

57. Swamydas, M., Bessert, D., and Skoff, R. (2009). Sexual dimorphism of oligodendrocytes is mediated by differential regulation of signaling pathways. J. Neurosci. Res. *87*, 3306–3319. https://doi.org/10.1002/jnr.21943.

58. Marin-Husstege, M., Muggironi, M., Raban, D., Skoff, R.P., and Casaccia-Bonnefil, P. (2004). Oligodendrocyte progenitor proliferation and maturation is differentially regulated by male and female sex steroid hormones. Dev. Neurosci. *26*, 245–254. https://doi.org/10.1159/000082141.

59. Nagy, C., Maitra, M., Tanti, A., Suderman, M., Théroux, J.F., Davoli, M.A., Perlman, K., Yerko, V., Wang, Y.C., Tripathy, S.J., et al. (2020). Single-nucleus transcriptomics of the prefrontal cortex in major depressive disorder implicates oligodendrocyte precursor cells and excitatory neurons. Nat. Neurosci. *23*, 771–781. https://doi.org/10.1038/s41593-020-0621-y.

60. Kokkosis, A.G., Madeira, M.M., Mullahy, M.R., and Tsirka, S.E. (2022). Chronic stress disrupts the homeostasis and progeny progression of oligodendroglial lineage cells, associating immune oligodendrocytes with prefrontal cortex hypomyelination. Mol. Psychiatry *27*, 2833–2848. https://doi.org/10.1038/s41380-022-01512-y.

61. Poggi, G., Albiez, J., and Pryce, C.R. (2022). Effects of chronic social stress on oligodendrocyte proliferation-maturation and myelin status in prefrontal cortex and amygdala in adult mice. Neurobiol. Stress *18*, 100451. https://doi.org/10.1016/j.ynstr.2022.100451.

62. Alonso, G. (2000). Prolonged corticosterone treatment of adult rats inhibits the proliferation of oligodendrocyte progenitors present throughout white and gray matter regions of the brain. Glia *31*, 219–231. https://doi.org/10.1002/1098-1136(200009)31:3<219::AID-GLIA30>3.0.CO;2-R.

63. Voskuhl, R.R., and Gold, S.M. (2012). Sex-related factors in multiple sclerosis susceptibility and progression. Nat. Rev. Neurol. *8*, 255–263. https://doi.org/10.1038/nrneurol.2012.43.

64. Willner, P. (2017). The chronic mild stress (CMS) model of depression: History, evaluation and usage. Neurobiol. Stress *6*, 78–93. https://doi.org/10.1016/j.ynstr.2016.08.002.

65. Dadomo, H., Gioiosa, L., Cigalotti, J., Ceresini, G., Parmigiani, S., and Palanza, P. (2018). What is stressful for females? Differential effects of

unpredictable environmental or social stress in CD1 female mice. Horm. Behav. *98*, 22–32. https://doi.org/10.1016/j.yhbeh.2017.11.013.

66. Karamihalev, S., Brivio, E., Flachskamm, C., Stoffel, R., Schmidt, M.V., and Chen, A. (2020). Social dominance mediates behavioral adaptation to chronic stress in a sex-specific manner. Elife *9*, e58723. https://doi.org/10.7554/eLife.58723.

67. Franceschelli, A., Herchick, S., Thelen, C., Papadopoulou-Daifoti, Z., and Pitychoutis, P.M. (2014). Sex differences in the chronic mild stress model of depression. Behav. Pharmacol. *25*, 372–383. https://doi.org/10.1097/FBP.0000000000000062.

68. Takele Assefa, A., Vandesompele, J., and Thas, O. (2020). On the utility of RNA sample pooling to optimize cost and statistical power in RNA sequencing experiments. BMC Genom. *21*, 312. https://doi.org/10.1186/s12864-020-6721-y.

69. Häusl, A.S., Brix, L.M., Hartmann, J., Pöhlmann, M.L., Lopez, J.-P., Menegaz, D., Brivio, E., Engelhardt, C., Roeh, S., Bajaj, T., et al. (2021). The co-chaperone Fkbp5 shapes the acute stress response in the paraventricular nucleus of the hypothalamus of male mice. Mol. Psychiatry *26*, 3060–3076. https://doi.org/10.1038/s41380-021-01044-x.

70. Lopez, J.P., Lücken, M.D., Brivio, E., Karamihalev, S., Kos, A., De Donno, C., Benjamin, A., Yang, H., Dick, A.L.W., Stoffel, R., et al. (2022). Ketamine exerts its sustained antidepressant effects via cell-type-specific regulation of Kcnq2. Neuron *110*, 2283–2298.e9. https://doi.org/10.1016/j.neuron.2022.05.001.

71. Chen, Z.-H., Li, S., Xu, M., Liu, C.C., Ye, H., Wang, B., and Wu, Q.-F. (2022). Single-cell Transcriptomic Profiling of the Hypothalamic Median Eminence during Aging. J. Genet. Genom. *49*, 523–536. https://doi.org/10.1016/j.jgg.2022.01.001.

72. Hasel, P., Rose, I.V.L., Sadick, J.S., Kim, R.D., and Liddelow, S.A. (2021). Neuroinflammatory astrocyte subtypes in the mouse brain. Nat. Neurosci. *24*, 1475–1487. https://doi.org/10.1038/s41593-021-00905-6.

73. McCarthy, M.M., Pickett, L.A., VanRyzin, J.W., and Kight, K.E. (2015). Surprising origins of sex differences in the brain. Horm. Behav. *76*, 3–10. https://doi.org/10.1016/j.yhbeh.2015.04.013.

74. Byers, S.L., Wiles, M.V., Dunn, S.L., and Taft, R.A. (2012). Mouse Estrous Cycle Identification Tool and Images. PLoS One *7*, e35538. https://doi.org/10.1371/journal.pone.0035538.

75. Schwanhäusser, B., Busse, D., Li, N., Dittmar, G., Schuchhardt, J., Wolf, J., Chen, W., and Selbach, M. (2011). Global quantification of mammalian gene expression control. Nature *473*, 337–342. https://doi.org/10.1038/nature10098.

76. Johnson, A., Rainville, J.R., Rivero-Ballon, G.N., Dhimitri, K., and Hodes, G.E. (2021). Testing the Limits of Sex Differences Using Variable Stress. Neuroscience *454*, 72–84. https://doi.org/10.1016/j.neuroscience.2019.12.034.

77. Péter, A. (2019). Solomon Coder.

78. R Core Team (2020). R: A Language and Environment for Statistical Computing.

79. Stuart, T., Butler, A., Hoffman, P., Hafemeister, C., Papalexi, E., Mauck, W.M., Hao, Y., Stoeckius, M., Smibert, P., and Satija, R. (2019). Comprehensive Integration of Single-Cell Data. Cell *177*, 1888–1902.e21. https://doi.org/10.1016/j.cell.2019.05.031.

80. Luecken, M.D., and Theis, F.J. (2019). Current best practices in single-cell RNA-seq analysis: a tutorial. Mol. Syst. Biol. *15*, e8746. https://doi.org/10.15252/msb.20188746.

81. Lun, A.T.L., McCarthy, D.J., and Marioni, J.C. (2016). A step-by-step workflow for low-level analysis of single-cell RNA-seq data with Bioconductor. F1000Res. *5*, 2122. https://doi.org/10.12688/f1000research.9501.2.

82. Soneson, C., and Robinson, M.D. (2018). Bias, robustness and scalability in single-cell differential expression analysis. Nat. Methods *15*, 255–261. https://doi.org/10.1038/nmeth.4612.

83. Finak, G., McDavid, A., Yajima, M., Deng, J., Gersuk, V., Shalek, A.K., Slichter, C.K., Miller, H.W., McElrath, M.J., Prlic, M., et al. (2015). MAST: a flexible statistical framework for assessing transcriptional changes and characterizing heterogeneity in single-cell RNA sequencing data. Genome Biol. *16*, 278. https://doi.org/10.1186/s13059-015-0844-5.

84. Krassowski, M., and CyrilLagger. (2021). Krassowski/Complex-Upset: v1.2.1. https://doi.org/10.5281/ZENODO.4718811.

85. Lex, A., Gehlenborg, N., Strobelt, H., Vuillemot, R., and Pfister, H. (2014). UpSet: Visualization of intersecting sets. IEEE Trans. Vis. Comput. Graph. *20*, 1983–1992. https://doi.org/10.1109/TVCG.2014.2346248.

86. Micallef, L., and Rodgers, P. (2014). eulerAPE: Drawing Area-Proportional 3-Venn Diagrams Using Ellipses. PLoS One *9*, e101717. https://doi.org/10.1371/journal.pone.0101717.

87. Wilkinson, L. (2012). Exact and approximate area-proportional circular venn and euler diagrams. IEEE Trans. Vis. Comput. Graph. *18*, 321–331. https://doi.org/10.1109/TVCG.2011.56.

88. Kuleshov, M.V., Jones, M.R., Rouillard, A.D., Fernandez, N.F., Duan, Q., Wang, Z., Koplev, S., Jenkins, S.L., Jagodnik, K.M., Lachmann, A., et al. (2016). Enrichr: a comprehensive gene set enrichment analysis web server 2016 update. Nucleic Acids Res. *44*, W90–W97. https://doi.org/10.1093/nar/gkw377.

89. Chen, E.Y., Tan, C.M., Kou, Y., Duan, Q., Wang, Z., Meirelles, G.V., Clark, N.R., and Ma'ayan, A. (2013). Enrichr: interactive and collaborative HTML5 gene list enrichment analysis tool. BMC Bioinf. *14*, 128. https://doi.org/10.1186/1471-2105-14-128.

90. Cahill, K.M., Huo, Z., Tseng, G.C., Logan, R.W., and Seney, M.L. (2018). Improved identification of concordant and discordant gene expression signatures using an updated rank-rank hypergeometric overlap approach. Sci. Rep. *8*, 9588. https://doi.org/10.1038/s41598-018-27903-2.

91. Plaisier, S.B., Taschereau, R., Wong, J.A., and Graeber, T.G. (2010). Rank-rank hypergeometric overlap: Identification of statistically significant overlap between gene-expression signatures. Nucleic Acids Res. *38*, e169. https://doi.org/10.1093/nar/gkq636.

92. Ximerakis, M., Lipnick, S.L., Innes, B.T., Simmons, S.K., Adiconis, X., Dionne, D., Mayweather, B.A., Nguyen, L., Niziolek, Z., Ozek, C., et al. (2019). Single-cell transcriptomic profiling of the aging mouse brain. Nat. Neurosci. *22*, 1696–1708. https://doi.org/10.1038/s41593-019-0491-3.

93. Cao, J., Spielmann, M., Qiu, X., Huang, X., Ibrahim, D.M., Hill, A.J., Zhang, F., Mundlos, S., Christiansen, L., Steemers, F.J., et al. (2019). The single-cell transcriptional landscape of mammalian organogenesis. Nature *566*, 496–502. https://doi.org/10.1038/s41586-019-0969-x.

94. Trapnell, C., Cacchiarelli, D., Grimsby, J., Pokharel, P., Li, S., Morse, M., Lennon, N.J., Livak, K.J., Mikkelsen, T.S., and Rinn, J.L. (2014). The dynamics and regulators of cell fate decisions are revealed by pseudotemporal ordering of single cells. Nat. Biotechnol. *32*, 381–386. https://doi.org/10.1038/nbt.2859.

95. Qiu, X., Mao, Q., Tang, Y., Wang, L., Chawla, R., Pliner, H.A., and Trapnell, C. (2017). Reversed graph embedding resolves complex single-cell trajectories. Nat. Methods *14*, 979–982. https://doi.org/10.1038/nmeth.4402.

96. Harris, C.R., Millman, K.J., van der Walt, S.J., Gommers, R., Virtanen, P., Cournapeau, D., Wieser, E., Taylor, J., Berg, S., Smith, N.J., et al. (2020). Array programming with NumPy. Nature *585*, 357–362. https://doi.org/10.1038/s41586-020-2649-2.

97. Pedregosa, F., Varoquaux, G., Gramfort, A., Michel, V., Thirion, B., Grisel, O., Blondel, M., Prettenhofer, P., Weiss, R., Dubourg, V., et al. (2011). Scikit-learn: Machine Learning in Python. J. Mach. Learn. Res. *12*, 2825–2830.

98. Rueden, C.T., Hiner, M.C., Evans, E.L., Pinkert, M.A., Lucas, A.M., Carpenter, A.E., Cimini, B.A., and Eliceiri, K.W. (2022). PyImageJ: A library

for integrating ImageJ and Python. Nat. Methods *19*, 1326–1327. https://doi.org/10.1038/s41592-022-01655-4.

99. Hoyer, S., and Hamman, J. (2017). xarray: N-D labeled Arrays and Datasets in Python. J. Open Res. Softw. *5*, 10. https://doi.org/10.5334/jors.148.
100. van der Walt, S., Schönberger, J.L., Nunez-Iglesias, J., Boulogne, F., Warner, J.D., Yager, N., Gouillart, E., and Yu, T.; scikit-image contributors (2014). scikit-image: image processing in Python. PeerJ *2*, e453. https://doi.org/10.7717/peerj.453.
101. Virtanen, P., Gommers, R., Oliphant, T.E., Haberland, M., Reddy, T., Cournapeau, D., Burovski, E., Peterson, P., Weckesser, W., Bright, J., et al. (2020). SciPy 1.0: fundamental algorithms for scientific computing in Python. Nat. Methods *17*, 352. https://doi.org/10.1038/s41592-020-0772-5.
102. McKinney, W. (2010). Data Structures for Statistical Computing in Python, pp. 56–61. https://doi.org/10.25080/Majora-92bf1922-00a.
103. The pandas development Team (2020). Pandas. Python Package. https://doi.org/10.5281/zenodo.3509134.
104. Longair, M.H., Baker, D.A., and Armstrong, J.D. (2011). Simple neurite tracer: Open source software for reconstruction, visualization and analysis of neuronal processes. Bioinformatics *27*, 2453–2454. https://doi.org/10.1093/bioinformatics/btr390.
105. Ferreira, T.A., Blackman, A.V., Oyrer, J., Jayabal, S., Chung, A.J., Watt, A.J., Sjöström, P.J., and Van Meyel, D.J. (2014). Neuronal morphometry directly from bitmap images. Nat. Methods *11*, 982–984. https://doi.org/10.1038/nmeth.3125.
106. Bates, D., Mächler, M., Bolker, B., and Walker, S. (2015). Fitting Linear Mixed-Effects Models Using lme4. J. Stat. Softw. *67*. https://doi.org/10.18637/jss.v067.i01.
107. Pinheiro, J., Bates, D., DebRoy, S., and Sarkar, D.; R Core Team (2020). Nlme: Linear and Nonlinear Mixed Effects Models.
108. Kuznetsova, A., Brockhoff, P.B., and Christensen, R.H.B. (2017). lmerTest Package: Tests in Linear Mixed Effects Models. J. Stat. Softw. *82*. https://doi.org/10.18637/jss.v082.i13.
109. Zucco, A.G. (2018). adrigabzu/sholl_analysis_in_R: AUC Calculation and Stats. https://doi.org/10.5281/ZENODO.1158612.
110. Wilson, M.D., Sethi, S., Lein, P.J., and Keil, K.P. (2017). Valid statistical approaches for analyzing sholl data: Mixed effects versus simple linear models. J. Neurosci. Methods *279*, 33–43. https://doi.org/10.1016/j.jneumeth.2017.01.003.
111. Ouyang, J.F., Kamaraj, U.S., Cao, E.Y., and Rackham, O.J.L. (2021). ShinyCell: simple and sharable visualization of single-cell gene expression data. Bioinformatics *37*, 3374–3376. https://doi.org/10.1093/bioinformatics/btab209.
112. RStudio Team (2019). RStudio: Integrated Development for R.
113. Wickham, H., Averick, M., Bryan, J., Chang, W., McGowan, L., François, R., Grolemund, G., Hayes, A., Henry, L., Hester, J., et al. (2019). Welcome to the Tidyverse. J. Open Source Softw. *4*, 1686. https://doi.org/10.21105/joss.01686.
114. Wickham, H. (2016). ggplot2: Elegant Graphics for Data Analysis Springer-Verlag.
115. Garnier, S. (2018). Viridis: Default Color Maps from "Matplotlib". R Package.
116. Lenth, R.V. (2021). Emmeans: Estimated Marginal Means, Aka Least-Squares Means.

STAR★METHODS

KEY RESOURCES TABLE

REAGENT or RESOURCE	SOURCE	IDENTIFIER
Antibodies		
Mouse Anti-Olig2 Monoclonal Antibody, Unconjugated, Clone 211F1.1	Millipore	Cat# MABN50; RRID:AB_10807410
Rabbit anti-Tmem10	Peles Laboratory, Weizmann Institute of Science (https://doi.org/10.1002/glia.20688)	N/A
Goat anti-Mouse IgG (H+L) Highly Cross-Adsorbed Secondary Antibody, Alexa Fluor™ Plus 488	Thermo Fisher Scientific	Cat# A32723; RRID:AB_2633275
Goat anti-Rabbit IgG (H+L) Highly Cross-Adsorbed Secondary Antibody, Alexa Fluor™ Plus 594	Thermo Fisher Scientific	Cat# A32740, RRID:AB_2762824
Chemicals, peptides, and recombinant proteins		
Modified Wright-Giemsa stain	Sigma Aldrich	Cat# WG16
Papain Dissociation System	Worthington BC	Cat# LK003163
Critical commercial assays		
Corticosterone Double Antibody RIA Kit	MP Biomedicals	Cat# 0712010-CF
Chromium™ Single Cell 3' Library Kit v2	10x Genomics	Cat# 120234
Chromium™ Single Cell 3' Gel Bead Kit v2	10x Genomics	Cat# 120235
Chromium™ Single Cell A Chip Kit	10x Genomics	Cat# 1000009
Chromium™ i7 Multiplex Kit	10x Genomics	Cat# 120262
RNAscope multiplex fluorescent reagent kit v1	ACD	Cat# 322340
RNAscope multiplex fluorescent reagent kit v2	ACD	Cat# 323110
Deposited data		
Raw sequencing data, aligned feature-barcode matrices from Cell Ranger and metadata matrix	This paper	GEO: GSE201032
Clustered dataset	This paper	https://male-female-stress.weizmann.ac.il/shinyApp/
Original R and Python code	This paper	https://github.com/EBrivio/sex_stress/
Experimental models: Organisms/strains		
Mouse: c57bl6/N wild-type	in-house breeding	N/A
Software and algorithms		
Cell Ranger	10x Genomics	RRID:SCR_017344
RStudio	http://www.rstudio.com	RRID:SCR_000432
R Project for Statistical Computing v. 3.6.3		RRID:SCR_001905
R package tidyverse v. 1.3.0	https://doi.org/10.21105/joss.01686	RRID:SCR_019186
R package ggplot2 v. 3.3.0	https://ggplot2.tidyverse.org	RRID:SCR_014601
R package viridis v. 0.5.1	https://cran.r-project.org/package=viridis	RRID:SCR_016696
R package ComplexUpset v. 1.2.0	https://doi.org/10.5281/ZENODO.4718811; https://doi.org/10.1109/TVCG.2014.2346248; https://cran.r-project.org/web/packages/ComplexUpset/index.html	RRID: SCR_022752
R package eulerr v. 6.1.0	https://doi.org/10.1371/journal.pone.0101717; https://doi.org/10.1109/TVCG.2011.56	RRID: SCR_022753
R package Seurat v 3.1.3	https://doi.org/10.1016/j.cell.2019.05.031	RRID:SCR_016341
R package scran v. 1.14.6	https://doi.org/10.12688/f1000research.9501.2	RRID:SCR_016944
R package: lme4 v. 1.1-26	https://doi.org/10.18637/jss.v067.i01	RRID:SCR_015654

(*Continued on next page*)

Continued

REAGENT or RESOURCE	SOURCE	IDENTIFIER
R package: lmerTest v. 3.1-3	https://doi.org/10.18637/jss.v082.i13	RRID:SCR_015656
R package: nlme v. 3.1-144		RRID:SCR_015655
R package emmeans v. 1.5.4		RRID:SCR_018734
R package RRHO2 v.1.0	https://doi.org/10.1038/s41598-018-27903-2; https://doi.org/10.1093/nar/gkq636	RRID:SCR_022754
R package Monocle3 v. 0.2.1	https://doi.org/10.1038/s41586-019-0969-x; https://doi.org/10.1038/nbt.2859; https://doi.org/10.1038/nmeth.4402	RRID:SCR_018685
R package Shiny v. 1.4.0.2		RRID:SCR_001626
R package ShinyCell v. 2.1.0	https://doi.org/10.1093/bioinformatics/btab209	https://github.com/SGDDNB/ShinyCell; RRID:SCR_022756
R package shinyhelper v. 0.3.2		RRID:SCR_022755
R package shinythemes v1.2.0		RRID:SCR_022757
Fiji v. 1.53c	https://doi.org/10.1038/nmeth.2019	RRID:SCR_002285
Simple Neurite Tracer v. 3.1.7	https://doi.org/10.1093/bioinformatics/btr390	RRID:SCR_016566
Sholl analysis v. 4.0.1	https://doi.org/10.1038/nmeth.3125	RRID:SCR_022758
Python v. 3.10.8	http://www.python.org/	RRID:SCR_008394
Python package jupyterlab v. 3.4.6	https://jupyter.org/	RRID:SCR_023339
Python package numpy v. 1.22.4	https://doi.org/10.1038/s41586-020-2649-2	RRID:SCR_008633
Python package tifffile v. 2022.8.12	https://doi.org/10.5281/zenodo.6795860	RRID:SCR_023338
Python package scikit-learn v. 1.1.1	http://scikit-learn.sourceforge.net	RRID:SCR_002577
Python package matplotlib v. 3.5.2	https://doi.org/10.1109/MCSE.2007.55	RRID:SCR_008624
Python package pillow v. 9.2.0	https://pillow.readthedocs.io/en/stable/	RRID:SCR_023337
Python package pyimagej v. 1.3.2 (initialization: sc.fiji:fiji, ImageJ2 v. 2.9.0/1.53t)	https://doi.org/10.1038/s41592-022-01655-4	RRID:SCR_023336
Python package scijava v. 1.8.1	https://scijava.org/	RRID:SCR_023335
Python package xarray v. 2022.12.0	https://doi.org/10.5334/jors.148	RRID:SCR_023334
Python package scikit-image v. 0.19.2	https://doi.org/10.7717/peerj.453	RRID:SCR_021142
Python package SciPy v. 1.7.3	https://doi.org/10.1038/s41592-020-0772-5	RRID:SCR_008058
Python package pandas v. 1.5.2	https://doi.org/10.5281/zenodo.3509134	RRID:SCR_018214
Python package findmaxima2d v. 0.0.25	https://pypi.org/project/findmaxima2d/	RRID:SCR_023332
Python package roifile v. 2022.7.29	https://doi.org/10.5281/zenodo.6941603	RRID:SCR_023331
R package pheatmap	https://www.rdocumentation.org/packages/pheatmap/versions/0.2/topics/pheatmap	RRID:SCR_016418
Solomon Coder v. 17.03.32	https://solomoncoder.com/	RRID:SCR_016041
Other		
RNAscope probe Mm-Gad1	ACD	Cat# 400951
RNAscope probe Mm-Gapdh-No-X-Hs-C2	ACD	Cat# 442871-C2
RNAscope probe Mm-Ndn-C3	ACD	Cat# 442711-C3
RNAscope probe Mm-Gas7	ACD	Cat# 518561
RNAscope probe Mm-Tspan2	ACD	Cat# 444741
RNAscope probe Mm-Mog-C2	ACD	Cat# 492981-C2
RNAscope probe Mm-Olig2-C3	ACD	Cat# 447091-C3

RESOURCE AVAILABILITY

Lead contact

Further information and requests for resources and reagents should be directed to and will be fulfilled by the lead contact, Alon Chen (alon.chen@weizmann.ac.il).

Materials availability

This study did not generate new unique reagents.

Data and code availability

- Raw sequencing data, aligned feature-barcode matrices from Cell Ranger and metadata matrix are accessible in the Gene Expression Omnibus (GEO) repository under the accession number GEO: GSE201032. An interactive web interface containing the clustered single cell dataset and metadata is available at: https://male-female-stress.shinyapps.io/shinyapp/.
- Adaptation and parameters of the standard available R packages such as Seurat and Monocle3 are available in the STAR Methods section. Statistical analysis of cell-cell interaction analyses has been adapted from Nagy et al.[44] as stated in the STAR Methods section.
- Original R scripts for ambient RNA calculations, clustering stability measurement, neuronal reclustering, distance calculation between stress backgrounds, oligodendrocyte DEGs clustering, pseudotime analysis and CCInx analysis, and original Python scripts for RNAscope image processing and analysis are collected at https://github.com/EBrivio/sex_stress/ and are publicly available as of the date of publication.
- Any additional information and code details are available from the lead contacts upon request.

EXPERIMENTAL MODEL AND SUBJECT DETAILS

Mice husbandry

Sexually-mature C57BL/6N mice, aged 7–10 weeks, were housed in same-sex pairs in individually ventilated cages with water and food *ad libitum* on a 12:12 h light-dark schedule in the animal facilities of the Max Planck Institute of Psychiatry in Munich, Germany. All experiments were approved by and conducted in accordance with the regulations of the local Animal Care and Use Committee (Government of Upper Bavaria, Munich, Germany). For the single cell RNA sequencing experiment, two cohorts of mice were used: cohort one received ARS under Baseline conditions (Baseline history); cohort two received ARS after CMS (CMS history).

For the estrus cycle monitoring, the vaginal opening of female mice was flushed with 1x PBS every morning for a minimum of 10 days. Samples were then dried at 37°C and stained with modified Wright-Giemsa stain (Sigma Aldrich, WG16-500ML). Estrus stage was assigned based on the relative amount of exfoliated vaginal cells (nucleated epithelial cells, cornified epithelial cells and leukocytes).[74] Males were handled on the same days to minimize confounding effects. Animals that did not show a regular cycle during these 10 days were excluded (Figures S1B and S1D). A non-regular cycle was defined as prolonged estrus (more than 5 days), prolonged diestrus (more than 5 days) or no estrus over the whole monitoring period.

METHOD DETAILS

Stressors

Unpredictable chronic mild stress (CMS)

For the study of the impact of a history of stress on the acute stress response, cages in the second cohort of mice were assigned to either the control or CMS group.

Each CMS cage received a random combination of two of the below stressors per day (one in the a.m. and one in the p.m. hours) for a total of 21 days.

1. Removal of nesting material (24 h);
2. Cage-tilt 30° along the vertical axis (6 h);
3. No bedding or nesting material (8 h);
4. Damp bedding (6 h, 200 ml of 23°C water mixed in the normal bedding);
5. Water avoidance (15 min): an empty rat cage (395 x 346 cm) was filled with room temperature water, mice were placed on a platform (10 x 12 cm), 2 cm above the water level;
6. Cage-change (4 h): mice received a fresh cage every 30 min for a total of 4 h;
7. Cage-switch: mice were assigned the cage of another group of the same sex;
8. Overcrowding (1 h): mice were placed with 8-10 same-sex stranger mice in a fresh cage;
9. Tail suspension (15 min): mice were hung by their tail, 50 cm above the surface for 15 min;
10. Homecage space reduction (6h): mice were left in ¼ of cage space for 6 h.

To assess the efficacy of the CMS paradigm, both stress and control animals were monitored twice per week for bodyweight and coat state. Their coat state was scored on a scale 0 to 3 according to the following criteria.

0) Shiny/well-groomed/healthy coat (no injuries or alopecia patches);
1) Less shiny/less groomed coat or small alopecia patches, but healthy (no wounds);

2) Dull coat and/or small wounds or alopecia patches;
2) Extensive piloerection or alopecia with crusted eyes or extensive wounds.

Cumulative coat state was calculated as the sum of the seven daily scores. Bodyweight gain was calculated as the difference of bodyweight at day 21 from day 1.

At sacrifice, adrenal glands were collected, isolated from connective and surrounding fat tissue, and weighed. A mean adrenal size per animal was calculated using both glands and normalized on bodyweight at sacrifice.

For each individual, bodyweight change, cumulative coat state, and mean normalized adrenal size were calculated and Z-scored (population of reference used was the whole dataset combined). Parameters were then directionally-normalized, so that positive values represented a stress state and negative value represented a non-stress state and summed to obtain the stress score.

Acute stress

Acute stress consisted of 15 min restraint in a ventilated tube in the dark around ~8:00 am. For the Baseline background, half of the mice were assigned to the stress group, for the CMS history, all stress mice also received ARS on Day 22.

Animals were sacrificed 5 hours after receiving the ARS, their brains collected, and were either flash frozen, perfused or processed for the scRNA-seq experiment. We selected a timepoint of 5 hours after stress in order to capture the second wave of transcription which peaks approximately around this time.[75] Bodyweight at sacrifice, trunk blood, and adrenals were also collected after the CMS paradigm.

Splash test (ST)

To validate the impact of CMS, a separate cohort of male and female mice underwent the chronic stress paradigm and 10 h after the end of the stress were tested[76] For this purpose, mice were tested in the splash test during the dark phase of the light cycle under dim illumination (~10-15lux).

Each animal was sprayed twice on the back (~500µl per spray) with a 10% sucrose solution and then placed in their original cage. Mice behaviour was recorder for 5[77] All tests and analysis were conducted by an experimenter blind to the sex and genotype of the mice.

Corticosterone assessment

A separate cohort of mice was used for corticosterone measurement. Mice were assigned either the Baseline background or the CMS background. On the day of the ARS, a few µl of tail blood were collected in EDTA-coated tubes right before the ARS and at the end of the 15 minutes of restraint. Blood was centrifuged at 1,000g for 15 min at 4°C. Plasma was retrieved and corticosterone levels were measured using [^{125}I] radioimmunoassay kit (MP Biomedicals), according to the manufacturer's instructions.

Single cell RNA-sequencing

Single cell suspensions

Single cell suspensions were prepared as previously described.[22] Briefly, five animals per conditions were sacrificed with a lethal dose of isoflurane and transcardially perfused in cold 1x PBS. One PVN-containing slice per animal (approximately -0.58mm Bregma to -1.22mm Bregma) was obtained using a 0.5 mm brain matrix and the extended PVN was manually dissected under the microscope (Figure S2A). For each condition, tissue was pooled and digested in Papain supplemented with DNase I at 37°C for 50 minutes. Tissue was then dissociated with a fire-polished glass pipette, filtered with a 30 µm strainer, and layered over a discontinuous density gradient of ovomucoid protease inhibitor with bovine serum albumin. All steps were executed in cold carbonated (95% O_2, 5% CO_2) artificial cerebrospinal fluid (aCSF: 87 mM NaCl, 2.5 mM KCl, 1.25 mM NaH_2PO_4, 26 mM $NaHCO_3$, 10 mM glucose, 75 mM sucrose, 2 mM Mg^{2+}, 1 mM Ca^{2+}). Cells were resuspended to a final concentration of ~700,000-900,000 cells/ml before being loaded on the 10x Genomics Chromium Controller, v2 chips, aiming at 10,000 cells per channel.

Library preparation and sequencing

Library was prepared using the 10x Genomics Single Cell 3' Reagent Kits v2 according to the manufacturer's protocol. Molar concentration and fragment length of libraries were quantified using Bioanalyzer (Agilent High Sensitivity DNA kit – N. 5067-4626) and samples within each background were pooled in equal molarity for sequencing. The pooled libraries were sequenced on a NovaSeq 6000 sequencer with paired-end asynchronous sequencing, 100 cycles with a depth of ~150 million reads per sample.

Pre-processing and quality control

Data was pre-processed with the 10x Genomics CellRanger software and further annotated on the mm10 reference set. Quality control, clustering and downstream analysis was performed within R version 3.6.3 (2020-02-29)[78] using the package Seurat v. 3.1.3,[79] following the guidelines provided by the developers and best practice workflow in single cell data analysis.[80] Briefly, putative dead cells, empty droplets, and multiplets were eliminated based on gene, UMI and mitochondrial gene counts (genes > 350 and < 3500, UMI < 15,000, and mitochondria < 30%), and the support of the functions *doubletCluster* and *doubletCells* from the package scran v. 1.14.6.[81] Blood cells were also considered as contaminants and removed from the dataset. This resulted in a dataset of 35,672 single cells with a median number of UMIs (unique molecular identifier) of 2,118, a median number of genes of 1,149, and median mitochondrial content of 0.045 per cell (Figures S1E and S1G).

Clustering

For clustering, data was log-normalized and scaled (factor 10,000) with the function *NormalizeData* in Seurat. The top 4,000 variable genes were selected using the function *FindVariableFeatures* in Seurat and used to scale the data with the function *ScaleData*. Twenty-two principal components and a resolution of 1.2 were used to cluster cells with the function *FindClusters*. Cells were than plotted in the ''Uniform Manifold Approximation and Projection'' (UMAP) bidimensional space and the identity of the cell clusters was identified overlapping known marker genes (Figure S1H) from literature over our clusters.[22] This identified 33 clusters belonging to 17 main cell types: neurons (GABAergic, glutamatergic, vasopressin, and mixed), astrocytes, microglia, macrophages, oligodendrocytes, committed oligodendrocytes progenitors (COPs), oligodendrocytes progenitor cells (OPCs), ependymal cells, tanycytes, endothelial cells, mixed endothelial cells, pericytes, vascular cells, meningeal cells. To better characterize the neuronal populations, the neuronal clusters (GABAergic, glut and mixed) were further c[17] First, we computed the number of PCs to use for reclustering by permutation analysis. For each group of cells, we created 50 different expression matrices by randomly permuted each row (gene) independently across cells (columns). For each matrix we then calculated the maximum eigenvalue from a PCA. As such, for downstream reclustering we selected all PCAs that had an eigenvalue higher than the mean of distribution of maximum eigenvalues obtained from the permutations. This analysis led us to recluster the GABAergic neurons with 32 PCs, glutamatergic neurons with 20 PCs, and mixed neurons with 18 PCs. Second, we clustered these three groups using the method explained above with the resolution that maximized the presence of stable clusters. To determine such resolution, we performed a subsampling analysis with 20 replicates. For each resolution tested (from 0.2 to 2.0), we selected a random 50% of cells and repeated the data scaling, identification of variable features, PCAs, the shared nearest neighbour graph from FindClusters and the cluster identification. We then checked which of the cells that clustered together in the full group consistently clustered together in the subsampled dataset. As such, for each original cluster we calculated the maximum fraction of cells that could be found in any subsampled clusters. The average of this value across the 20 replicates was used as a metrics of cluster stability. All our clusters resulted stable (average > 0.5), as such, we selected the resolution parameter that maximized this stability value (GABA: 0.4, glut: 0.2, mixed: 0.2).

Marker genes for each cluster were identified using the function *FindAllMarkers* and *FindMarkers* with default settings (Table S1).

Ambient RNA calculations

Raw matrices obtained from Seurat were used to calculate the average Ambient RNA contaminations. For each sample we identified the pool of empty droplets containing contaminant RNA (approximately 100 genes and less than 150 molecules per droplet). Selected droplets were used to calculate the average expression of all genes with the function AverageExpression. The complete list is available in Table S2.

Differential gene expression analysis

Differential gene expression analysis was performed using MAST[82,83] integrated in the function *FindMarkers* of Seurat to identify genes that were different between stress (either ARS under Baseline or ARS under CMS conditions) and control within the same sex for each of the clusters. To avoid ambient RNA noise, we tested only genes expressed in at least 50% of cluster cells in either condition. BH-adjusted p values less than 0.05 were used to determine significantly deregulated genes. Furthermore, average gene expression per cluster was calculated using *AverageExpression* function on log-normalized scaled data. Graphical representation of DEGs was done producing either Upset plots (R package ComplexUpset v.1.2.1[84,85]) or Venn Diagrams (R package eulerr v.6.1.0[86,87]). To assess the similarity of the ARS response between male and female, the Szymkiewicz–Simpson coefficient was calculated according to its formula: (N. of intersecting genes)/(N. of DEGs of the smallest responder for each pair).

To identify the enrichment for transcription factors interacting with the DEGs from Baseline ARS shared between the sexes, the 137 DEGs were inputted in the online platform Enrichr.com [88,89] using the ''Transcription Factor PPIs'' function which uses a literature-based protein-protein interaction network to identify enrichment for transcription factors interactors. Results are reported in term of p value, network and clustergram.

Euclidean distance

Background influence on acute stress response was assess describing each cell cluster by the number of DEGs and the median absolute log fold change of DEGs. Distance between ARS under CMS and Baseline was calculated as euclidean distance between the two datapoints for each sex. Distances have been Z-scored within each sex and summed between male and female, to evaluate which cell type was the most affected across sexes.

RRHO analysis

For the rank-rank hypergeometric overlap (RRHO) analysis on the differentially expressed transcriptome of male and female cell types (oligodendrocytes, glutamatergic neurons, and astrocytes), we used the R package RRHO2 v.1.0[90,91] for each sex on all genes present in both conditions. Each gene was inputted as the product between its p value * the sign of the fold change.

Hierarchical clustering

To identify subgroups of genes with similar patterns of regulation across conditions, a hierarchical clustering analysis was performed on all genes that showed differential expression in at least one condition in oligodendrocytes. To do so, we first created a matrix containing all these genes and their logFC. Genes that were not tested in a condition were assigned 0. We than calculated their Euclidean distance on the scaled distance matrix. Based on the highest agglomerative coefficient score, Ward's methos was selected as the clustering method and the R function hclust from the stats package was used to perform the clustering. Finally, based on clustering

results, the dendrogram was cut to generate 16 clusters (k = 16). The heatmap was constructed using the R package pheatmap v.1.0.12.

Cell-cell interaction analysis

@To evaluate predicted cell–cell interaction networks, we used predicted ligand–receptor interactions between oligodendrocytes and neurons using the package CCInx v. 0.5.1 (baderlab.github.io/ccinx/).[92] The package uses the Cell-Cell interaction database (http://baderlab.org/CellCellInteractions) to quantify ligand-receptor interactions as edge weights. We calculated the networks within each of our eight samples (namely Control and ARS for each condition: Baseline Female, Baseline Male, CMS Female, CMS Male) for all genes with expression value higher than 1.5. To evaluate how much stress exposure perturbates interaction networks, a delta edge weight was calculated within each condition as (edge weight stress – edge weight control). Delta edge weights < 0.01 were removed and we performed a permutation analysis based on Nagy et al.[59] to test which changes in edge weight were significantly different. More specifically, we randomly permuted our control and stress cells into two groups for 100 times and calculated the distribution of edge weight differences between the two groups for each of our ligand-receptor pair. We then calculated a p-value for each of our stress-control edge weight differences and applied the BH post-hoc p-value correction across all test runs. Edge weight with q-value <0.05 were considered significant. To evaluate if stress impacted the ligand-receptor networks in a directionality-specific way, the distribution of edge weights of deregulates receptor-ligands pairs for either direction (oligodendrocytes to neuron, and neuron to oligodendrocyte) were explored. The analysis was performed between each pair of oligodendrocytes and neuronal clusters (GABA, glut, AVP, mixed) separately (Figure S4A) to maintain possible neuron-specific interactions. All neuronal pairs showed similar distributions and were finally aggregated to increase power.

Pseudotime analysis

To study the developmental trajectory of the oligodendrocytes, we isolated the clusters belonging to the oligodendrocyte lineage (COP, OPC and Oligodendrocytes) and re-clustered them within Seurat v. 3.1.3 with the same procedure explained above, 15 PCs and a resolution of 0.6. The Seurat object was then transformed into a Monocle3's object by importing the gene expression matrix, cell metadata, and UMAP coordinates.[93–95]

To construct ethe single-cell pseudotime trajectory of oligodendrocytes,[93–95] we first built a trajectory graph with the function learn_graph. In order to place each cell on this trajectory, we assigned the root to the far-left node, as this was populated by OPC cells (Figure 5A, circled one). Cells were then ordered based on their assigned pseudotime value and their distribution compared between conditions. Cells projection over pseudotime was presented both as density plots and cumulative plots. Statistical analysis was run on the cumulative curves for each control-stress pair using a two-sample, two-sided Kolmogorov-Smirnov test with BH p-value adjustments.

RNAscope

Staining

To validate gene expression changes in GABAergic neurons and oligodendrocytes, we performed RNAscope on selected genes. Fresh frozen brains, four per conditions, were sliced in a cryostat at a thickness of 10μm. Two sections approximately 200μm apart containing the PVN were collected per animal. Sections were processed with RNAscope multiplex fluorescent reagent kit (v1: GABAergic neurons ACD, Cat. N. 322340; v2: oligodendrocytes - ACD, Cat. N. 323110) according to manufacturer's protocol. The following combination of probes and fluorophores were used.

Probe	Fluorophore
Mm-Gad1 (N. 400951)	Alexa-488
Mm-Gapdh-No-X-Hs-C2 (N. 442871-C2)	Atto550
Mm-Ndn-C3 (N. 442711-C3)	Atto647
Mm-Gas7 (N. 518561)	Opal570
Mm-Tspan2 (N. 444741)	Opal570
Mm-Mog-C2 (N. 492981-C2)	Opal520
Mm-Olig2-C3 (N. 447091-C3)	Opal690

Oligodendrocytes genes were processed in the following order: Mog – Olig2 – Gas7 or Tspan2. Slides were mounted with ProLong Gold Antifade Mountant (Thermo Fisher Scientific, Cat. N. P36930) and imaged as tiled 8-field pictures (2048 x 2048 resolution, 40x objective, 0.24 μm z-stack) at a Leica DMi8 spinning disk (pinhole size 40 μm) confocal microscope.

Image analysis

To quantify RNA scope staining we used a custom script written in Python v. 3.10.8 and Fiji v. 1.53t. The following Python modules were used: jupyterlab v. 3.4.6, numpy v. 1.22.4[96,97] matplotlib v. 3.5.2 (Hunter, 2007), pillow v. 9.2.0, pyimagej v. 1.3.2 (initialization: sc.fiji:fiji, ImageJ2 version: 2.9.0/1.53t),[98] scijava v. 1.8.1, xarray v. 2022.12.0,[99] scikit-image v. 0.19.2,[100] scipy v. 1.7.3,[101] pandas v. 1.5.2,[102,103] findmaxima2d v. 0.0.25, roifile v. 2022.7.29. All the hyperparameters of the analysis were determined manually, blind to

the experimental groups, in order to optimize the different steps of the protocol. The same hyperparameters were applied to the data when experimental groups were to be compared. First, DAPI signal was rescaled over the 16-bit value range and purposely saturated by setting all pixels whose values were in the upper 90th percentile to the 16-bit maximum value. We then applied edge-preserving image smoothing, Otsu threshold and watershed and removed areas smaller than 40 pixels. The obtained binary mask was then imported in Fiji and used to automatically recognize cell areas. In order to collect the whole cellular signal, nuclear shapes were expanded to generate the analyzed region of interest (ROIs), as follows. Binary masks were first converted to 8-bit depth and the Voronoi map for each field was obtained with the voronoi function. Each voronoi cell was then labelled and expanded of 35 pixels in all directions by a circle-shaped structuring element. The PVN was manually labelled based on anatomical references and cell ROIs outside the PVN were discarded.

For each cell we then computed the nucleus size, the cell size, the number of puncta and the average radius of puncta. Puncta were identified exploiting a blob detection function based on the Laplacian of Gaussian method, built-in in Python's scikit-image module. We first rescaled all channels independently over the 16-bit value range, by using the tissue background intensity value and the maximum value respectively as the lower and upper extremes of the rescaling range. The intensity value of background tissue was estimated as the mode of the signal intensity histogram, after removing the intensity value of the ventricle (visible in all the analyzed pictures). The following parameters were then used to detect blobs: min_sigma 1, max_sigma 8, num_sigma 4, overlap 0.9. A single threshold value was manually determined per each RNA probe, blind to the experimental conditions, and used for all samples.

Cells were defined outliers and removed if their nucleus or area size fell outside the median ± 1.5 interquartile range (IQR). To determine if a cell was positive to a cell marker (either *Gad1*, *Mog* or *Olig2*), we calculate an expression value by multiplying the number of puncta by their average radius and split its distribution by k-means clustering. For Gad1 signal we assumed the possibility of binary identity, either positive or negative, as such the clustering was performed with k = 2. For *Mog* and *Olig2*, given the existence of varying levels of expression and their sparse expression, we assumed four (k = 4) different groups: no expression (negative), background expression (negative), low expression (positive), high expression (positive). For all downstream analysis, the value of puncta in each cell was used as measure of signal.

Morphology analysis of oligodendrocytes

For oligodendrocytes morphology analysis, a cohort of male and female mice received ARS after CMS, as previously described. Five hours after the end of ARS, mice were lethally anesthetized in isoflurane and transcardially perfused in 4% PFA. Brains were collected, post-fixated in 4% PFA for 24 h at 4°C and then moved to 30% sucrose until sinkage. Two 40 μm-sections containing the PVN (one frontal and one caudal, 200 μm apart) per animal were processed for immunofluorescence. Briefly, tissue was blocked in blocking solution (5% normal goat serum, 0.5% Triton X-100 in 1x PBS) for 1 h at room temperature. Primary antibodies (α-Tmem10, rabbit, 1:500 (provided by Prof. Elior Peles, Weizmann Institute of Science, Israel), α-olig2, mouse, 1:250 (Millipore MABN50)) were then incubated at 4°C for 20 h in blocking solution. Secondary antibodies (α-Rabbit-Alexa Fluor488 1:500 and α-Mouse-Alexa Fluor 594 1:500)) were further incubated at room temperature for 1 h. Slides were mounted with DAPI Fluoromount-G (SouthernBiotech, Cat. N. 0100-20).

In each slide, left and right PVN were acquired as a tiled 4-field picture (1024 x 1024 resolution, 40x objective, 0.5x magnification, 2 μm z-stack) at a LSM800 Zeiss confocal microscope.

For tracing, the PVN region was first defined based on DAPI density. All visible Tmem10+, Olig2+ cells within the defined PVN were labelled and the Tmem10 signal was traced using the Fiji plugin Simple Neurite Tracing v.3.1.7[104] by an experimenter blind to the sex and condition. Sholl analysis was performed on the traces obtained using the plug-in Sholl analysis v. 4.0.1 available in Fiji[105] with default parameters and continuous sampling from the centre of soma. Concentric intersections were binned to intervals of 5 μm. To remove intersections due to soma crossing, soma radius was calculated from its circumference and any intersections with a radius < soma radius were removed. In addition to the intersection distribution, we calculated the maximal distance from the soma for each cell. Statistical analysis was performed applying a nested design within a mixed-effects models with the R package lme4 v. 1.1-26,[106] nlme v. 3.1-144[107] and lmerTest v.3.1-3[108] based on the implementation in R of sholl analysis.[109,110] For each condition, 6 animals were used with an average of 14.29 cells per animal. Representative cells in Figure 5E were generated using the skeletonize function within Simple Neurite Tracer.

QUANTIFICATION AND STATISTICAL ANALYSIS

Data manipulation and statistical analysis have been performed within R studio v. 1.2.5033[112] with R version 3.6.3 (2020-02-29)[78] and the support of the package tidyverse v. 1.3.0.[113]

Plots were generated using the R package ggplot2 v. 3.3.0[114] and viridis v. 0.5.1[115] if not differently specified before.

ANOVAs, linear models and post-hoc p-value corrections have been computed using the packages lme4 v. 1.1-26,[106] nlme v. 3.1-144,[107] lmerTest v. 3.1-3,[108] and emmeans v. 1.5.4,[116] as stated for each result. When ANOVA was used, Shapiro-Wilk normality test was used to verify normality in data distribution. In case normality was violated (as in coat state data distribution) non-parametric test such as Kruskal-Wallis rank sum test were used.

ADDITIONAL RESOURCES

Web app

The Shiny-based web interactive app containing the processed and clustered dataset was created using the R package ShinyCell v. 2.1.0.[111] The loaded object available in the app includes all detected genes and all metadata (i.e., sample, cohort, condition, n. UMIs, n. detected genes, % mitochondrial genes, clusters, cell types). The app is available at https://male-female-stress.weizmann.ac.il/shinyApp/ as of the date of publication.